Line Shapes in Electron Spin Resonance

Charles P. Poole and Horacio A. Farach
Department of Physics and Astronomy
University of South Carolina
Columbia, SC 29208, USA

I. INTRODUCTION

Most treatments of "static" electron spin resonance (ESR) emphasize the positions and spacings of spectral lines and the interpretation of these quantities in terms of Hamiltonian parameters. "Dynamic" ESR studies are concerned with the measurement of relaxation times and the explanation of relaxation processes in terms of microscopic mechanisms. For many systems, the shapes and widths of ESR spectral lines contain a considerable amount of information on both static and dynamic aspects of the spin system.

The purpose of the present review is to survey the types of lineshapes encountered in practice and to show how to extract from them information on the Hamiltonian parameters and environmental interactions of the paramagnetic species.

Typical ESR spectra consist of multiplets arising from the superposition of individual lines which are Gaussian or Lorentzian in shape. High viscosity liquids tend to produce Lorentzian lines, dipolar broadening in solids is characterized by Gaussian shapes, and exchange narrowing causes lines to be Lorentzian in the center and Gaussian in the wings. These shapes will be defined analytically in the next two sections.

If the interactions which produce the ESR spectra are directionally dependent, then the appearance of the spectrum will vary with the orientation of the magnetic field relative to the crystallographic axes. If the sample is a powder or a glass, then the spectra arising from various orientations will be superimposed and produce a powder pattern without angular dependence. In low viscosity fluids, the anisotropies will largely average out to produce a spectrum arising from the isotropic parts of the interactions. At high viscosities, spectra are complex and only partially averaged.

This review will discuss the lineshapes arising from these and other cases. The emphasis will be on surveying the different lineshapes that arise in solid and liquid phases, rather than on providing exhaustive coverage of the literature. The lineshapes characteristic of specialized systems such as triplet states, conduction electrons, magnetically and electronically ordered systems, and one and two dimensional cases will be treated in a later review.

II. SHAPES AND MOMENTS

An absorption spectral line $Y(H)$ can be characterized by the values of its various moments

$$<H^n> = \frac{1}{A}\int_{-\infty}^{\infty}(H - H_o)^n\, Y(H)\, dH \qquad (1)$$

where A is the area under the absorption curve

$$A = \int_{-\infty}^{\infty} Y(H)\, dH \qquad (2)$$

and H_o is defined as the magnetic field value which makes the first moment vanish

$$<H^1> = \frac{1}{A}\int_{-\infty}^{\infty}(H - H_o)\, Y(H)\, dH = 0 \qquad (3)$$

For first derivative lines

$$Y'(H) = \frac{dY(H)}{dH} \qquad (4)$$

we have the corresponding expressions

$$<H^n> = -\frac{1}{(n+1)A}\int_{-\infty}^{\infty}(H - H_o)^{n+1}\, Y'(H)\, dH$$

$$0 = \int_{-\infty}^{\infty} Y'(H)\, dH \qquad (5)$$

$$A = -\int_{-\infty}^{\infty}(H - H_0)\, Y'(H)\, dH$$

$$<H^1> = \frac{1}{2A}\int_{-\infty}^{\infty}(H - H_o)^2\, Y'(H) \qquad dH=0$$

The second of these expressions is the condition for the proper choice of the baseline, and the fourth is the condition for the proper choice of H_o. Analogous expressions can be written for second derivative presentation (1).

In addition to its moments, an absorption line has a full width $\Delta H_{1/2}$ between the half-amplitude points, and a first derivative absorption line has a full peak-to-peak width ΔH_{pp} between maximum positive and negative deflections,as indicated respectively on Figures 1 and 2. It

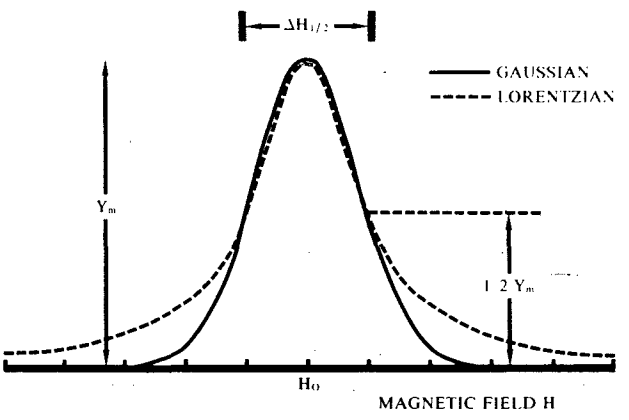

Figure 1. Comparison of Gaussian and Lorentzian absorption lineshapes.

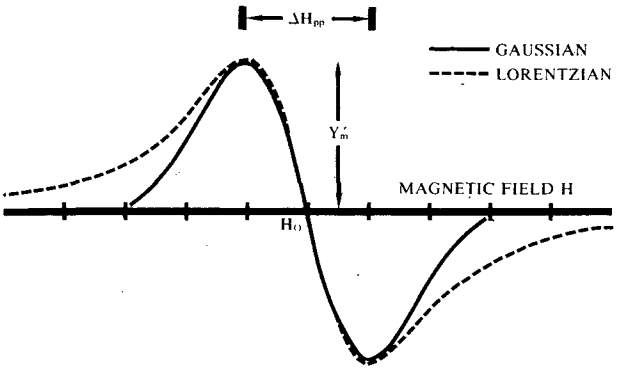

Figure 2. Comparison of Gaussian and Lorentzian first-derivative absorption lineshapes.

is convenient to employ normalized moments, $<H^n>/(\Delta H_{1/2})^n$ for the absorption line case, and $<H^n>/(\Delta H_{pp})^n$ for the first derivative line case.

For symmetrical lines, all odd moments vanish and all even moments exist. For a Gaussian shape

$$Y(H) = y_m \exp\left[-\left(\frac{H - H_o}{\frac{1}{2}\Delta H_{1/2}}\right)^2 \ln 2\right] \qquad (6)$$

or its derivative

$$Y'(H) = e^{1/2}\, y'_m \left(\frac{H - H_o}{\frac{1}{2}\Delta H_{pp}}\right) \exp\left[-\frac{1}{2}\left(\frac{H - H_o}{\frac{1}{2}\Delta H_{pp}}\right)^2\right] \qquad (7)$$

the moments are given by

$$<H^n> = 0 \qquad n \text{ odd} \qquad (8)$$

and

$$<H^n> = (n-1)!!\,(\tfrac{1}{2}\Delta H_{pp})^n \qquad n \text{ even} \qquad (9)$$

where the symbol $(n-1)!! = (n-1)(n-3)\ldots 5 \cdot 3 \cdot 1$.
A Gaussian shape has the particular parameters

$$\Delta H_{1/2} = (2 \ln 2)^{1/2}\, \Delta H_{pp} = 1.1776\, \Delta H_{pp}$$

$$A = \frac{1}{2}(\pi/\ln 2)^{1/2}\, \Delta H_{1/2} y_m = 1.0643\, H_{1/2}\, y_m$$

$$= \tfrac{1}{4}(2\pi e)^{1/2}(\Delta H_{pp})^2\, y'_m = 1.0332(\Delta H_{pp})^2\, y'_m \qquad (10)$$

$$y_m = \tfrac{1}{2}e^{1/2}\, \Delta H_{pp}\, y'_m = 0.8244\, \Delta H_{pp}\, y'_m$$

$$<H^2> = \tfrac{1}{4}(\Delta H_{pp})^2 = 0.2500(\Delta H_{pp})^2$$

$$<H^4> = \frac{3}{16}(\Delta H_{pp})^4 = 0.1875(\Delta H_{pp})^4 \qquad (11)$$

For a Lorentzian shape

$$Y(H) = \frac{y_m}{1+(H-H_o)^2/(\frac{1}{2}\Delta H_{\frac{1}{2}})^2} \qquad (12)$$

and its derivative

$$Y'(H) = \frac{16\, y'_m\left(\frac{H-H_o}{\frac{1}{2}\Delta H_{pp}}\right)}{\left[3+\left(\frac{H-H_o}{\frac{1}{2}\Delta H_{pp}}\right)^2\right]^2} \qquad (13)$$

we have the expressions

$$\Delta H_{\frac{1}{2}} = 1.7321\,\Delta H_{pp}$$

$$A = \frac{\pi}{2}\Delta H_{\frac{1}{2}}\, y_m = 1.5708\,\Delta H_{\frac{1}{2}}\, y_m$$

$$= \frac{2\pi}{\sqrt{3}}(\Delta H_{pp})^2 y'_m = 3.6276(\Delta H_{pp})^2\, y'_m \qquad (14)$$

$$Y_m = 1.3333\,\Delta H_{pp}\, y'_m$$

Since the shape is symmetrical, all odd moments vanish. The wings of a Lorentzian line converge so slowly that all even moments are infinite.

Sometimes it is useful to work with a lineshape that is almost Lorentzian in the center and has a finite second moment. One such shape is the cut-off Lorentzian which is Lorentzian in the range

$$(H_o - a) \leq H \leq (H_o + a) \qquad (15)$$

about the center field H_0 and is zero outside this range. All even moments are finite and have closed-form expressions (1,2). Another such shape is the square Lorentzian

$$Y(H-H_o) = \frac{y_m}{[1+(H-H_o)^2\Gamma^2]^2} \qquad (16)$$

which has a finite second moment and infinite fourth and higher-order even moments (3).

The degree of asymmetry of a resonance line may be measured by the magnitudes of its odd moments, and a simple parameter to characterize such asymmetry is the ratio of the cube root of the third moment to the square root of the second moment, $\langle H^3\rangle^{\frac{1}{3}} / \langle H^2\rangle^{\frac{1}{2}}$. Svare (4) calculated this ratio for dipolar coupled spins at low temperature and obtained a finite value, which indicates that the lineshape is not symmetrical.

The shapes of experimental spectra can be conveniently checked to ascertain if they are Lorentzian or Gaussian (1). It has been customary to calculate moments from experimental spectra by numerical or graphical methods. Rakos et al (5) have described an analogue electronic device for the automatic computation of second moments.

Work up to 1967 on the use of moments in analyses of ESR line shapes was summarized by Poole (1). Buluggiu et al (6) discussed the effect of covalence on moments. Wenzel (7) obtained an expression for the second moment of ESR lines broadened by strong hyperfine or superhyperfine interactions. O'Reilly and Tsang (8) employed lattice harmonics to analyze line shapes. Lin and Kevan (9) determined the differences between the second moments of trapped electrons in sodium ice condensates with and without deuteration at 9 and 35 GHz, and thereby obtained the isotropic and anisotropic hyperfine coupling constants of the nearest neighbor protons.

III. LINEWIDTH ANISOTROPY

Van Vleck (10) showed that the width of an ESR absorption line depends on orientation and that its variation with direction depends on the crystal structure. In many cases, this width variation is much less than the width itself, and hence is not noticeable experimentally. A number of authors (11-48) have studied the angular dependence of the width, and typical results are listed in Table 1.

Sastry and Sastry (39) explained the linewidth anisotropy of Cu^{2+} in a tetramine thiocyanate complex in terms of contributions from dipolar (ΔH_{dd}), hyperfine (ΔH_{hf}), and exchange (H_{exch}) interactions. Their expression for the linewidth ΔH is

$$\Delta H_{\frac{1}{2}} = 2\left(\frac{10}{3}\Delta H_{dd}^2 + \Delta H_{hf}^2\right) / H_{exch} \qquad (17)$$

For the case of tetragonal symmetry, Sastry and Sastry used the following expression from Bleaney et al (49)

$$\Delta H_{hf}^2 = K(1 + 3\cos^2\phi) \qquad (18)$$

where ϕ is the angle between the applied magnetic field and the tetragonal axis. The dipolar contribution ΔH_{dd} is also orientation dependent.

IV. CONVOLUTIONS

When a spectral line is broadened independently by both Gaussian and Lorentzian effects, then the lineshape is a convolution obtained by integrating the product of the lineshapes, equations (6) and (12). If the full half-amplitude Gaussian and Lorentzian widths, respectively, are denoted by $G_{\Delta H_{\frac{1}{2}}}$ and $L_{\Delta H_{\frac{1}{2}}}$ then the lineshape is given by (1)

Table 1. Selected Reports on Lineshape and Linewidth Anisotropies

Paramagnetic Species	Host	Graph of ΔH vs Angle	Comments	Reference
radical	irradiated bone	no	quasirandom distribution	11
radical	TMPD chloranil	yes	dipolar anisotropy	12
radical	irradiated Na acetate	no	anisotropy due to shifts	13
radical	naphthalene	yes	triplet pairs	14
CO_2^-	$CaCO_3$	yes	tunneling	15,16
CF_2CONH_2	trifluoroacetamide		ΔH depends mainly on M_I^2	17
BrO_3^{2-}	$KBrO_3$	yes	uses jump model	18
centers	ZrO_2, HfO_2	no	77 K, irradiated	19
F center	KCl	no	experiment and theory	20
V_K center	KCl:Li	no	ΔH for many samples	21,22
VO_2^{2+}	$VO_2(NO_3)_2 \cdot 6H_2O$		300 K rapid reorientation	23
VO_6	V_2MoO_8	yes	e-hopping process	24
Cr^{3+}	MgO	yes	strain-modulated ESR	25
Cr^{3+}	Al_2O_3 (ruby)	no	$\Delta H_\perp$ homogenous, $\Delta H_\parallel$ inhomogeneous	26-28
Cr^{3+}	Al_2O_3 (ruby)	no	shape, width, equality	29
Cr^{3+}	$ZnWO_4$	yes	studies Li^+, Na^+ charge compensation	30,31
Cr^{3+}	alum	no	lineshape angle-dependent	32
Fe^{3+}	$ZnWO_4$	yes	concentration dependence	33,34
Mn^{2+}	$(NH_4)_2Ni(SeO_4)_2 \cdot 6H_2O$	no	ΔH field-dependent	35
Mn^{2+}	$Mg(HCOO)_2 \cdot 2H_2O$	yes	2-dimensional system	36
Mn	Si surface		Mn adsorbed	37
Mn^{2+}	$(NH_4)_2Ni_2(SO_4)_3$	no	Mn^{2+}-Ni^{2+} cross relaxation	38
Cu^{2+}	$Cu(trien)(SCN)_2$		width due to exchange, dipolar, and hyperfine contributions	39
Cu	Si surface	no	Cu adsorbed	37
Cu^{2+}	$Cu[OC(NH_2)NHNH_2]Cl_2$	yes	studies exchange; determines τ_c	40
Cu^{2+}	$Cu(NH_3)_2(CH_3COO)_2$	yes	different sites, weak exchange	41
Er	Ag film on NaCl	yes	space-dependent strain	42
Gd	LaSb	yes	$\Delta H = A + B(4\text{-}20x^2 + 15x^4)^2$ where $x = \sin\theta$	43
Gd	Y-Al-garnet	no		44
Gd	Y-Gd alloy	yes	explains anisotropy	45
Yb^{3+}	ZnS (sphalerite)	yes	asymmetry due to stacking faults	46
Y	$Y(C_2H_5SO_4)_3 \cdot 9H_2O$	yes	ΔH changes by factor of approximately 10	47
Pu^{3+},Am^{4+}	ThO_2, $SrCl_2$	no	ΔH anisotropic	48

$$Y(H) = \frac{(\ln 2)^{1/2}}{\pi} \left(\frac{L_{\Delta H_{1/2}}}{G_{\Delta H_{1/2}}} \right) \text{times the integral} \quad (19)$$

$$\int_{-\infty}^{\infty} \frac{e^{-x^2} dx}{\left(\frac{L_{\Delta H_{1/2}}}{G_{\Delta H_{1/2}}} \right)^2 \ln 2 + \left[2(\ln 2)^{1/2} \frac{H - H_o}{G_{\Delta H_{1/2}}} - x \right]^2}$$

where

$$x^2 = 2\left(\frac{H - H_o}{G_{\Delta H_{pp}}} \right)^2 \quad (20)$$

The integral (19) cannot be integrated in closed form, but Posener (50) has published tabulations of it. Castner (51) evaluated $Y(H)$ in terms of the error-function integral and described how to determine the linewidth ratio $L_{\Delta H_{1/2}} / G_{\Delta H_{1/2}}$. Farach and Teitelbaum (52) also showed how the Gaussian and Lorentzian widths may be determined.

The convolution lineshape has been employed to treat the case of inhomogeneous broadening with narrow Lorentzian spin packets forming a broader Gaussian-shaped envelope (see Section VI).

Gaussian-Lorentzian convolution lineshapes were also discussed by Strandberg (53), who gave new mathematical properties of the integral, and by Stoneham (54), who derived an expression for the relationship of the observed peak-to-peak linewidth ΔH_{pp} to the Gaussian and Lorentzian widths. Al'tshuler et al (55) used a convolution for the profile of the ESR line from localized spins in metals, and Kemple and Stapleton (56) employed it to explain the shape of Ho^{3+} in yttrium ethyl sulfate (YES).

V. EXCHANGE

A number of workers (57–60) have discussed theoretical aspects of how the exchange interaction influences ESR line shapes. Some of the recent experimental data obtained with exchange-dominated systems are summarized in Table 2.

Salikhov et al (62) presented a theory and experimental verification involving exchange broadening in dilute solutions containing free radicals with spin $S_1 = ½$ and paramagnetic complexes of transition ions with spin $S_2 \geq ½$. They assume exchange $J(t)$ to be operative only for the duration τ_c of a collision

$$J(t) = J \quad t_o \leq t \leq t_o + \tau_c \quad (21)$$

$$J(t) = 0 \quad t < t_o, \quad t > t_o + \tau_c \quad (22)$$

where t_o is the time for the start of the collision. The authors present tables of phase changes and efficiencies of collisions for spin lattice relaxation times that are long and short compared with τ_c.

Heinzer (68) employed the density matrix theory in the Liouville approximation to derive the following general first derivative lineshape formula for the case of intramolecular exchange between many sites

$$\frac{dy}{dw} = -\, I_m \left[\sum_j \sum_\mu s_{j\mu} (\Lambda_{j\mu} + iw)^{-2} \right] \quad (23)$$

where the imaginary part of $\Lambda_{j\mu}$ provides the line position, the real part of $S_{j\mu}$ is a measure of the intensity and the real part of $2\Lambda_{j\mu}/\sqrt{3}$ is the width of the line $j\mu$. The imaginary part of $\Lambda_{j\mu}$ produces a deviation from a Lorentzian shape. A computer program provides synthesized spectra from equation (23). More recently, Heinzer (69) applied a least-squares procedure to the computer analysis of isotropic-exchange-broadened ESR lineshapes.

Fedders (84) calculated spin-pair correlation functions for exchange narrowing using a microscopic derivation and a sum-rule moment expansion. The sum-rule method gave a frequency dependent linewidth. Theory was compared with experimental results on Rb MnF_3.

Boucher (102) showed that exchange-narrowed lines are essentially composed of the Fourier transforms of cross-correlation functions, while motionally-narrowed lines contain only the Fourier transform of the self-correlation function.

Myles (103) treated the case of anisotropic exchange energy J together with uniaxial anisotropy energy D. They examined the dependence of the dipolar spectral function, quadrupolar spectral functions, exchange-narrowed dipolar linewidths and spin-diffusion coefficients as a function of the spin S and the ratio $3D^2/16S(S+1)J^2$.

Cusumano et al (71,104) studied solid solutions of diphenyl picrylhydrazyl (DPPH) in polystyrene and found that the exchange-narrowed shapes are Lorentzian in the center and exponential in the wings. The experimental behavior resulted from the spin-lattice relaxation in this Heisenberg ferromagnet. Lazuta and Maleev (105) studied the dynamics of an impurity spin in a dielectric and also found an exponential lineshape. Misra et al (106-108) found that the linewidth in DPPH depends upon the recrystallization solution.

Most calculations of linewidths by the Van Vleck (10) moment method make use of a truncated Hamiltonian which excludes weak, subsidiary spectral lines at the positions 0, $2g\beta H_0$ and $3g\beta H_0$. These lines are not observed at high fields, but do contribute to the even moments and, in particular, increase the second

Table 2. Exchange Effects on ESR Linewidths and Lineshapes

System	State	Comments	Reference
$S = 1/2$, radical $S > 1/2$, paramagnetic metal ion	solution	mutual, linear concentration broadening	61,62
carbazyl	solution	applies Kivelson (1960) theory	63
phthalocyanine dye	solution	intramolecular exchange	64,65
K tetracyanoethylene	solution	slow and fast exchange	66
piperidine radical	solution	mixed with $Cu(NO_3)_2$	67
radical ion	solution	theory, calculated spectra	68,69
$(CH_3)_3COPH_3$	matrix	mobility, proton exchange	70
DPPH in polystyrene	powder	Lorentzian shape at center, exponential in wings	71
^{14}N in diamond	solid	exchange broadening	72
naphthyl-n-alkanes	polymer	inter- and intramolecular exchange in biradical	73,74
nitroxide, verdazyl, and hydrazyl radicals	solid	exchange-energy varied exponentially with spin separation	75
nitroxyl radicals	crystal	width due to weak exchange with non-nearest neighbors	76
TMPD chloranil	crystal	ΔH angular dependence follows 2nd moment of e-dipolar interaction	
Wurster's blue perchlorate	powder and single crystals	temperature-dependent exchange anisotropy; observed 10/3 effect	77
$Cr^{3+}/ZnGa_2O_4$	single crystal	pairs; isotropic, biquadratic, anisotropic exchange	78
Cr carboxylate	solid	3-ion clusters	79-82
tetramethyl Mn chloride		treats exchange narrowing mechanically without experimental verification	59
$Mn(TCNQ)_2$,$Mn(TCNQ\text{-}d_x)_2$	polycrystalline	AFM Mn^{2+} coupling	83
$RbMnF_3$	solid	calculates exchange narrowing	84
CuMn	alloy	theoretical explanation, conduction ESR	85
CuMn, AgMn	alloy	local moments	86
Ag, Mn/Sb, Au	alloy	HFS, exhange narrowing, dilute	87
$NiSiF_6 \cdot 6H_2O$	single crystal	temperature dependence, uniaxial anisotropy	88,89
$Cu(HCOO)_2 \cdot 4H_2O$	solid	temperature dependence, antisymmetric exchange	90
Cu^{2+} complexes	solid	dipolar and exchange interactions	91
Cu^{2+} chelate	solution, glass	monomer, dimer	92
Cu^{2+} oxalate	powder	amine complexes	93
$K_2CuCl_4 \cdot 2H_2O$	single crystal	J strongly temperature dependent	94
$Cu(NH_3)_4PtCl_4$	single crystal	exchange-narrowed Lorentzian; observed 10/3 effect; 1-dimensional exchange	95
$Eu_xM_{1-x}O$, $Eu_xM_{1-x}S$ ($M = Co^{2+}, Sr^{2+}, Ba^{2+}$)	solid	300 K, indirect exchange	96
EuS	film	spin-wave absorption, ferromagnetic resonance	97
Gd in Au	single crystal	local moments, high concentration, exchange narrowing	98
Gd_xY_{1-x}(P, As, Sb) and $Gd_xY_{1-x}Sb$	powders	Lorentzian center, asymmetric wings	99
Gd/(RE)F_3	single crystal	exchange causes ΔH to depend on M	100
Dy, Er, Yb in Ag, Al	alloy	ΔH calculation, anisotropic exchange	101

moment by the factor of 10/3 when the measurements are carried out at low frequencies. A number of authors have observed this 10/3 effect (see Table 2).

VI. INHOMOGENEOUS BROADENING

Homogeneous broadening occurs for a transition between two spin levels that are somewhat broadened rather than sharply defined. This type of broadening arises from the dipolar interaction between like spins, spin lattice relaxation, motional narrowing, and other effects. An inhomogeneously broadened line consists of a spectral distribution of individual resonant lines or spin packets merged into one overall line or envelope. Inhomogeneous broadening may be due to magnetic field nonuniformities, unresolved fine or hyperfine structure, and dipolar interaction between unlike spins.

Inhomogeneous broadening was analyzed by Portis (109,110) and Castner (51); their results were discussed in earlier reviews (1,111) and will not be repeated here. Castner analyzed the case of a Gaussian envelope of width $G_{\Delta H_{1/2}}$ composed of Lorentzian-shaped spin packets of width $L_{\Delta H_{1/2}}$, and he obtained the convolution lineshape of equation (19). He presented graphs which may be employed to determine the ratio $G_{\Delta H_{1/2}}/L_{\Delta H_{1/2}}$. In using this article, one should be careful to note the use of unconventional linewidth definitions. Coffman (112) analyzed inhomogeneously broadened high-spin Fe^{3+} spectra from biological specimens by making use of multiple contour integrals.

Cullis (113) treated inhomogeneously broadened lines in terms of a spin temperature in the rotating coordinate frame associated with the spin packets. He obtained expressions which describe the system for both slow and fast passage conditions, and his treatment reduced to Castner's results (51) in several cases.

The relaxation parameter of spin packets can be measured by the continuous saturation and spin echo methods. Semenov and Fogel'son (114) showed that an investigation of the dependence of the response signal on the intensity and duration of a saturating microwave pulse yields the saturation factor and width ($1/T_2$) of the spin packets that make up inhomogeneous lines.

Baumberg et al (115) found coherence effects in the inhomogeneous lines of nitrogen in SiC irradiated with a microwave pulse of duration less than T_2. This pulse burns a primary hole at the point of application, and smaller holes appear equally spaced and symmetrically arrayed about the primary hole. These arise from the rotation of spin-packet magnetization vectors by the coherent microwave pulses.

Epifanov and Manenkov (116) examined relaxation processes in inhomogeneously broadened lines by a quantum statistical method. Bugai (117) studied passage effects and Zhidkov et al (118) used continuous saturation to determine the width of the distribution function.

At liquid helium temperature, the $1/2 \leftrightarrow -1/2$ absorption line of Cr^{3+} in dilute ruby is found to be inhomogeneously broadened when the external magnetic field H_0 is directed along the c axis, and is homogeneously broadened when the external field is perpendicular to this axis (26-28). The broadening arises from superhyperfine structure from ^{27}Al nuclei which become magnetically equivalent in groups when H_0 is along c, and which generate spectral spin diffusion in the electron Cr^{3+} spin system, and hence increase the width.

Vugmeister et al (119) asserted that inhomogeneous broadening is characterized by interactions which lack dynamic terms, i.e., terms which cause energy exchange between different spins. The dynamic portion of the dipolar interaction produces homogeneous broadening when the energy exchange between separate spins occurs more rapidly than spin-lattice relaxation. For the case $g_{\parallel} > g_{\perp}$, with H_0 along the symmetry axis, the dynamic part of the interaction may be negligible, producing inhomogeneous broadening. At sufficiently low temperature, the homogeneity will be angularly dependent.

Mailer et al (120), analyzed the theoretical and experimental effects of radio-frequency (RF) and modulation field nonuniformities and sample length on the continuous-wave (CW) saturation characteristics of inhomogeneously broadened lines. They presented curves of signal-amplitude dependence on various parameters, and illustrated their results with experimental data on biological samples.

Strandberg (53) has treated correlation-time narrowing and narrowing by spin-stirring experiments with inhomogeneously broadened lines. He also elucidated relaxation and adiabatic fast-passage behavior.

Bowman et al (121) analyzed the saturation behavior of an inhomogeneously broadened line with second harmonic detection under slow-passage conditions. They presented curves which allow one to extract the width and relaxation times T_1 and T_2 from saturation data on inhomogeneous lines.

Inhomogeneously broadened lines are readily studied by electron-electron double resonance (ELDOR) in which one part of the line can be saturated and another observed. See Kevan and Kispart (122).

VII. POWDER PATTERNS

Until now the discussion has centered around spectra obtained from single crystals. We have seen how the position and width of a resonant line can depend upon the direction of the applied magnetic field relative to the crystallographic axes. It is best to obtain angular rotation data with single crystals if they are available, since such data will maximize the information attainable on the principal values and direction cosines of the Hamiltonian parameters.

However, sometimes single crystals are not available and it is necessary to work with powders, which have randomly oriented paramagnetic centers. In this case, the single crystal spectrum must be averaged over all angles to produce a powder-pattern spectrum with a shape characteristic of the Hamiltonian parameters. In section VIII, we will discuss in turn powder patterns arising from an axially symmetric Hamiltonian, totally unsymmetric cases, partially ordered or semi-random systems, and situations such as those that arise in glasses where the paramagnetic ions occupy sites with a range of Hamiltonian parameters. Several authors (1,42,123) have reviewed powder-pattern lineshapes. Table 3 summarizes some experimental results.

To illustrate the principles involved in the calculation of lineshapes from randomly oriented or powder samples, we consider the case of a single line arising from an angularly dependent g-factor

$$E = h\nu = g(\theta,\phi)\mu_\beta H' \qquad (24)$$

where θ and ϕ are the polar angles of the magnetic field

Table 3. Powder-pattern Reports in Chronological Order

Symmetries			Lineshape	Comments	References
g-factor *g*	Hyperfine *A*	Zero-field *D*	δ—delta function L—Lorentzian G—Gaussian		
axial	—	—	δ		49,124,125
asymmetric	—	—	δ	NMR	126
axial	—	—	δ		127
isotropic	—	axial	δ	spin = 3/2	128
asymmetric	—	—	δ		129
axial	axial	—	δ		130
axial	—	—	L,G	orientation-dependent transition probability	131,132
asymmetric	—	—	δ		133
isotropic	asymmetric	—	δ,G	good graphs	134
isotropic	asymmetric	—	G		135
isotropic	asymmetric	—	δ	spin = ½, nuclear Zeeman *I* = ½	136
asymmetric	—	—	L		137
axial	axial	—	G		138
asymmetric	—	—	—		135
axial	—	—	L	spin > ½, orientation-dependent transition probability	136a
isotropic	anisotropic	—	δ,G		137a
axial	axial	—	δ,G		138a
isotropic	asymmetric	—	G		139
axial	—	—	—		140
axial	—	—	L	orientation-dependent transition probability	141
axial	—	—	δ		142
isotropic	isotropic	—	δ,L		143
axial	axial	—	L,G		144
isotropic	—	—	G	orientation-dependent transition probability	145
asymmetric	asymmetric	—	L,G		146

Continued on next page

Table 3. Powder-pattern Reports in Chronological Order *(Continued)*

Symmetries			Lineshape	Comments	References
g-factor *g*	Hyperfine *A*	Zero-field *D*	δ—delta function L—Lorentzian G—Gaussian		
asymmetric	—	—	L,G	computer calculation	147
axial	axial	—	G		148
axial	—	—	arbitrary		149
axial	axial	—	L,G		150
asymmetric	—	—	L	valid for small anisotropy	151
asymmetric	asymmetric	—	—	large ^{19}F anisotropy	152
asymmetric	asymmetric	—	—	nuclear Zeeman $I = ½$	153
asymmetric	—	—	L		154
axial	anisotropic	—	—	computer simulation	155
axial	axial	—	L	orientation-dependent transition probability	156
isotropic	axial	—	δ	spin = ½, nuclear Zeeman $I = ½$, orientation-dependent transition probability	157
axial	—	—	L,G	shape-transform graph	158
—	asymmetric	—	—	discusses singularities	159,160
axial	—	asymmetric	—	spin = 3/2, no orientation-dependent transition probability, central powder pattern folded back	161,162
asymmetric	—	—	—	g_z/g_x vs g_x/g_y, orientation-dependent transition probability	163
axial	axial	—	L	different principal directions, orientation-dependent transition probability	164
axial	axial	—	L,G	quadrupole, nuclear Zeeman	165
isotropic	isotropic	axial	—	spin = 5/2, doubling gives signs	166
isotropic	axial	—	G	^{14}N HFS axial; rotating methyl group	167,168
isotropic	—	axial	δ	spin > ½	169,170
asymmetric	—	—	—	ΔH angular dependence	171,172
isotropic	—	—	δ	$H = \beta J \cdot g \cdot H + \alpha \sum J_i H_j E_k$ $(i \neq j \neq k)$ Stark term	173
axial	axial	—	L,G	spin = ½, vanadyl	174
asymmetric	asymmetric	—	G	nuclear Zeeman + asymmetric quadrupole	175
isotropic	—	asymmetric	G	spin = 5/2; includes B_4^M zero field	176
isotropic	—	axial	—	spin = 1, O_2 libration	177,178
asymmetric	—	asymmetric	—	spin = 1, different principal directions	179
asymmetric	—	asymmetric	δ	spin > ½	180
asymmetric	—	asymmetric	G	spin = 5/2, $g\beta H < D$	181
asymmetric	—	—	G	spin = ½; $I_1 = I_2 = ½$; torsional-oscillation axis distribution	182
axial	axial	—	δ	$I_1 = I_2 = I_3 = ½$, extra singularities	81,82,183
axial	axial	—	—		184
isotropic	—	asymmetric	—	spin = 5/2, g vs $3E/D$ plot	185

H' in the principal axis system of the g-tensor. Since the experiment is carried out at a constant frequency ν, we equate $h\nu$ to the product g_oH_o of a mean or average g-factor g_o and resonant field H_o

$$h\nu = g_o\mu_\beta H_o \tag{25}$$

The resonant field $H'(\theta,\phi)$ corresponding to the direction θ, ϕ is obtained by combining equations (24) and (25) and rearranging terms

$$H'(\theta,\phi) = \frac{H_o g_o}{g(\theta,\phi)} \tag{26}$$

The angularly dependent g-factor $g(\theta,\phi)$ may arise from an anisotropic Zeeman term, or, in a more general case, it may arise from an effective g-factor which includes zero-field interactions. If the spectrum consists of widely separated lines, then equation (26) applies to each, with $g(\theta,\phi)$ being different for each line. For simplicity, we now confine our attention to the spectrum of a single line and will treat hyperfine structure later.

If a study is made of a single crystal with one angularly dependent spectral line arising from equation (26), then the shape of the spectral line recorded at the orientation θ, ϕ will be

$$\text{Single-crystal lineshape} = P(\theta,\phi)\, Y\left(\frac{H - H'(\theta,\phi)}{\Delta H(\theta,\phi)}\right) \tag{27}$$

The lineshape function $Y\left(\frac{H - H'}{\Delta H}\right)$ in particular cases may indicate a Lorentzian or Gaussian absorption or derivative lineshape defined by equation (6), (7), (12), or (13), and the function $P(\theta,\phi)$ takes into account the angularly dependent probability that the microwave field will induce an ESR transition. In the general case, the transition probability P, the linewidth ΔH, the line shape function Y, and the resonant field position H are all angularly dependent. In most cases encountered in practice, the shape and width may be treated as constants independent of the orientation.

For a powder sample in which the microcrystallites are randomly oriented, the powder-pattern lineshape can be obtained by integrating equation (27) over a unit sphere

$$\text{Powder-pattern lineshape} = \int_o^{\pi}\int_o^{2\pi} P_{(\theta,\phi)}\, Y\left(\frac{H - H'(\theta,\phi)}{\Delta H(\theta,\phi)}\right) \sin\theta\, d\theta d\phi \tag{28}$$

In general, this is not a convenient expression to work with because H' is a complex function of position and is not easy to integrate. Some authors have simplified it for special cases, as discussed below. Taylor and Bray (186) have discussed the use of perturbation techniques in simulating powder spectra.

VIII. AXIAL POWDER PATTERNS

In the case of axial symmetry, there is no ϕ dependence and the single-crystal and powder-pattern lineshapes reduce to

$$\text{Single-crystal lineshape} = P_{(\theta)}\, Y\left(\frac{H - H'(\theta)}{\Delta H(\theta)}\right)$$

$$\text{Powder-pattern lineshape} = \int P_{(\theta)}\, Y\left(\frac{H - H'(\theta)}{\Delta H(\theta)}\right) \sin\theta\, d\theta \tag{29}$$

The g-factor has the explicit form

$$g = (g_\parallel^2\cos^2\theta + g_\perp^2\sin^2\theta)^{1/2} \tag{30}$$

which gives for H' of equations (29)

$$H' = \frac{g_o H_o}{(g_\perp^2 + (g_\parallel^2 - g_\perp^2)\cos^2\theta)^{1/2}} \tag{31}$$

The field H' varies with the angle θ between the limiting values $H_\parallel$ and $H_\perp$ given by

$$g_\parallel H_\parallel = g_\perp H_\perp = g_o H_o \tag{32}$$

where $H' = H_\parallel$ for $\theta = 0$ and $H' = H_\perp$ for $\theta = \pi/2$.

To transform equations (29) to more convenient forms, it is desired to convert them from functions of θ to functions of H'. To accomplish this, we observe that the probability of finding a microcrystallite randomly oriented at an angle θ is proportional to the area $\sin\theta\, d\theta$ of an annular ring about the pole of a unit sphere. Associated with the range of angles from θ to $\theta + d\theta$ is a range of resonant magnetic field strengths from H' to $H' + dH'$. The probability $G(H')$ of finding a microcrystallite which is resonant within this range is obtained from the expression

$$G_{(H')}\, dH' = \sin\theta\, d\theta = d(\cos\theta)$$

which may be written

$$G_{(H')} = \frac{1}{dH'/d(\cos\theta)} \tag{33}$$

Carrying out the differentiation of equation (31), we obtain

$$G_{(H')} = \frac{H_\parallel^3}{H'^2}\left(\frac{g_\parallel^2 - g_\perp^2}{g_\parallel^2 H_\parallel^2 - g_\perp^2 H'^2}\right)^{1/2} \tag{34}$$

which includes a normalization factor to make $G_{(H')} = 1$ for $H = H_\parallel$.

The transition probability for a linearly polarized oscillatory microwave field normalized to $P_{(H')} = 1$ for $\theta = 0$ corresponding to $H' = H_\parallel$ is given by (125)

$$P_{(H')} = \tfrac{1}{2}\left[\frac{H'^2}{H_\parallel^2} + 1\right] \tag{35}$$

As Table 3 indicates, many authors neglect this factor, which is equivalent to setting $P_{(H')} = 1$.

The single-crystal and the powder-pattern lineshapes are given by

$$\begin{aligned}\text{Single-crystal lineshape} &= P_{(H')}\, G_{(H')}\, Y\left(\frac{H - H'}{\Delta H}\right) \\ \text{Powder-pattern lineshape} &= \int_{H_\parallel}^{H_\perp} P_{(H')}\, G_{(H')}\, Y\left(\frac{H - H'}{\Delta H}\right) \mathrm{d}H'\end{aligned} \tag{36}$$

With the aid of equations (34) and (35), the latter expression may be put in the form

$$\text{Powder-pattern lineshape} = \frac{H_\parallel (g_\parallel^2 - g_\perp^2)^{1/2}}{2} \int_{H_\parallel}^{H_\perp} \frac{(H'^2 + H_\parallel^2)\, Y_{(H')}\, \mathrm{d}H'}{(g_\parallel^2 H_\parallel^2 - g_\perp^2 H'^2)^{1/2}} \tag{37}$$

where the limits of integration were selected for the case $H_\parallel < H_\perp$. For the opposite case $H_\perp < H_\parallel$, the integration limits are interchanged.

The general features of the lineshapes' angular dependence can be readily grasped by considering the special case of intrinsically narrow single-crystal lines, which corresponds to writing $Y_{(H')}$ as a delta function $\delta(H - H')$

$$\begin{aligned}\text{Delta-function lineshape} &= \int_{H_\parallel}^{H_\perp} P_{(H')}\, \delta_{(H - H')}\, G_{(H')}\, \mathrm{d}H' \\ &= P_{(H)}\, G_{(H)} \\ &= \frac{H_\parallel}{2H^2}\,(H^2 + H_\parallel^2)\left(\frac{g_\parallel^2 - g_\perp^2}{g_\parallel^2 H_\parallel^2 - g_\perp^2 H^2}\right)^{1/2}\end{aligned} \tag{38}$$

This lineshape exists within the range $H_\parallel \leq H \leq H_\perp$ (or $H_\perp \leq H \leq H_\parallel$) and vanishes outside it. Thus, the integrand $P_{(H')}\, G_{(H)}$ is often referred to as the delta-function lineshape. Many of the published lineshape articles have dealt only with delta-function shapes, as shown in Table 3.

Figure 3 shows the powder lineshapes for the cases of a delta-function width and a finite angularly independent

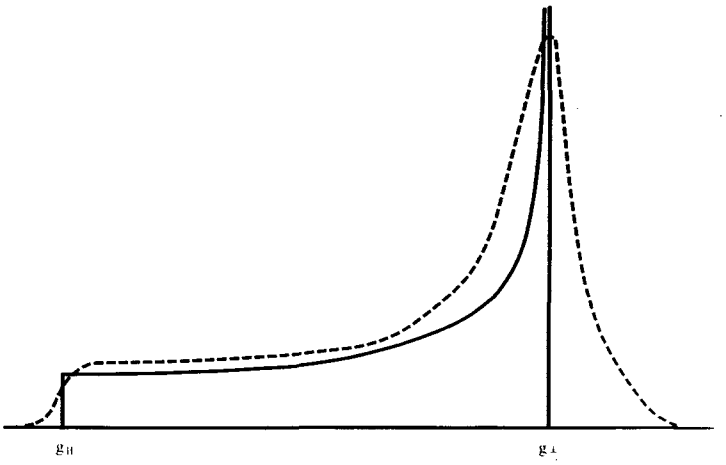

Figure 3. Powder-pattern absorption lineshapes for an axially symmetric g-factor. Component linewidth is zero for solid line, finite for dashed line.

width. A number of authors have treated this case of an axial g-factor, as Table 3 indicates. We see from the table that they generally set $P_{(H')} = 1$, and they rarely take into account an angularly dependent linewidth. Some of the articles in the table analyze cases of more complicated Hamiltonians which include hyperfine structure or zero-field terms. These latter cases involve the superposition of more than one line in the spectrum, and the resulting powder pattern can be written as the sum of the patterns of the individual component lines.

$$\text{Powder pattern} = \sum_i \int_{H_i}^{H_i} P_i(H')\, Y_i\left(\frac{H - H'}{\Delta H_i(H')}\right) G_i(H')\, \mathrm{d}H' \tag{39}$$

In general, each component can have its own characteristic functions P_i, Y_i, ΔH_i, and G_i, but in practice, Y_i and ΔH_i are generally the same for each component, and often one sets each P_i equal to unity.

The powder-pattern problem for an axially symmetric Hamiltonian with hyperfine structure corresponds to the following Hamiltonian (124,130,169)

$$\begin{aligned}h\nu = \beta(g_\parallel H_z S_z + g_\perp (H_x S_x + H_y S_y) + A_\parallel S_z I_z \\ + A_\perp (S_x I_x + S_y I_y)\end{aligned} \tag{40}$$

In terms of the parameter K defined by (124)

$$K^2 = \frac{g_\parallel^2 A_\parallel^2 \cos^2\theta + g_\perp^2 A_\perp^2 \sin^2\theta}{h^2\nu^2 (g_\parallel^2 \cos^2\theta + g_\perp^2 \sin^2\theta)} \tag{41}$$

$G_{(H)}$ for the mth hyperfine component has the form

$$G_{(H)} = \frac{g_o^2 H_o^2}{H^3(g_\parallel^2 - g_\perp^2)\cos\theta\left[1 + m\left(\frac{g_\parallel^2 A_\parallel^2 - g_\perp^2 A_\perp^2}{K(g_\parallel^2 - g_\perp^2)h^2\nu^2} - 2K\right)\right]} \quad (42)$$

If the individual component lines have finite widths, then the powder pattern is given by inserting $P_{(H')} = 1$ and $G_{(H')}$ from equation (42) into equation (36). Figure 4 shows the powder pattern arising from one hyperfine component in this axial case.

Shteinshneider and Zhidomirov (164) discussed the lineshapes obtained from a generalization of the Hamiltonian, equation (40), to the case where the g-factor and hyperfine tensors are axially symmetric with different principal directions. Various aspects of axial powder patterns in the presence of hyperfine structure have been treated by others (cf. Table 3).

Other Hamiltonian terms can also give axially symmetric powder patterns, such as a nuclear electric quadrupole moment. We have shown elsewhere that a zero-field D term $\vec{S}\cdot\overleftrightarrow{D}\cdot\vec{S}$ with a magnitude small relative to the Zeeman energy, produces the following delta-function lineshape when g is isotropic, $S \geq \frac{1}{2}$, and no hyperfine structure is present (169)

$$G_{(H)} = \sqrt{3}\left[\frac{2(H_o - H)}{nD} + 1\right]^{-\frac{1}{2}} \quad (43)$$

where D is in gauss, we assume $P_{(H')} = 1$, and

$$H_o = H + \frac{nD}{2}(3\cos^2\theta - 1) \quad (44)$$

Here n takes on the following sequence of values: $\pm(2S-1)$, $\pm(2S-3)$, . . . , ± 1 or 0, starting with the highest pair $\pm(2S-1)$ and decreasing in steps of 2 to the lowest value of 1 or 0. Thus, for example, for $S = 3/2$, we have $n = 0, \pm 2$, and for $S = 2$, we have $n = \pm 1, \pm 3$. The magnetic field produces resonant absorption between the limits (169)

$$-1 \leq \frac{2(H_o - H)}{nD} \leq 2$$

with $G_{(H)} = 1$ at the right hand limit and ∞ at the left hand limit, as may be shown by direct substitution in equation (43). When there is a finite component width, then $G_{(H)}$ integrates to a finite area in equation (43).

Mialhe et al (166) analyzed the powder pattern of Mn^{2+} in an axially symmetric environment in terms of a Hamiltonian with an isotropic g-factor and hyperfine interactions and an axially symmetric zero-field D term. The probability function $G_{(H)}$ for the lineshape has the usual infinity for $\theta = \pi/2$, where $\cos\theta = 0$, but in this case, it has another infinity at θ corresponding to the condition

$$8\cos^2\theta\left(1 + \frac{8A}{H_o}M_I + \frac{3A^2}{4DH_o}M_I\right) = \sin^2\theta\left(1 - \frac{6A^2}{DH_o}M_I\right) \quad (45)$$

which was obtained from perturbation theory. The result was a doubling of the allowed transitions which permitted the determination of the relative signs of the A and D tensors. Their spectra also exhibited forbidden lines between the main hyperfine components.

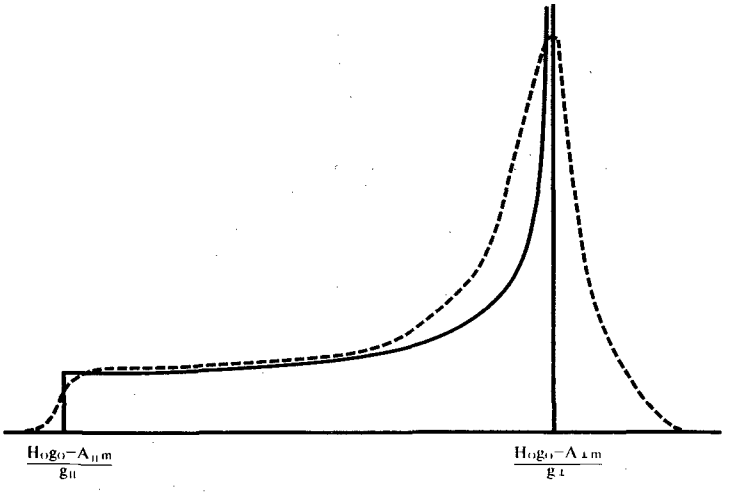

Figure 4. Powder-pattern absorption lineshapes for one component of a hyperfine multiplet when the g-factor and hyperfine tensors have the same axis of symmetry (from reference 1). Component linewidth is zero for the solid line, finite for the dashed line.

IX. COMPLETELY ANISOTROPIC POWDER PATTERNS

This section is concerned with Hamiltonians which lack symmetry so that tensor operators such as $\overleftrightarrow{g}$, $\overleftrightarrow{A}$, and $\overleftrightarrow{D}$ have three principal values. We will begin with a system which has only a Zeeman interaction but also complete asymmetry. Table 3 lists articles which treat powder patterns formed from various combinations of Hamiltonian terms some or all of which are completely anisotropic.

For the case of a completely anisotropic g-factor, equation (36) is still valid and now the angular dependence contains the two polar angles θ and ϕ

$$g = (g_1^2\sin^2\theta\cos^2\phi + g_2^2\sin^2\theta\sin^2\phi + g_3^2\cos^2\theta)^{\frac{1}{2}} \quad (46)$$

This expression reduces to equation (30) for axial symmetry where $g_1 = g_2$. The resulting lineshape for the convention

$$g_3 < g_2 < g_1 \quad (47)$$

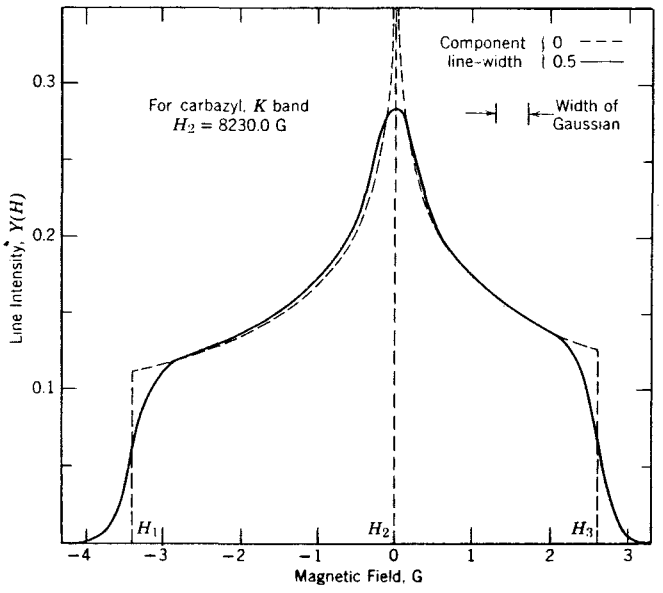

Figure 5. Calculated powder-pattern lineshape for carbazyl, assuming both zero and nonzero component linewidths (from references 1, 129).

which corresponds to

$$H_1 < H_2 < H_3 \qquad (48)$$

is illustrated in Figure 5. We see from the figure that there is an infinity at the magnetic field position $H_2 = h\nu/g_2\mu_\beta$, and this infinity integrates to a finite area. The delta-function lineshape corresponds to the probability $G_{(H)}$ which was introduced in the previous section, and when a finite linewidth exists, the lineshape $Y_{(H)}$ is calculated from equation (36). The transition probability $P_{(H)}$ for this case has been reported (163,188,189). Hauser and coworkers (171,172) calculated the powder pattern arising from a completely anisotropic g-factor when the component linewidth is also angularly dependent (see Table 3).

Table 3 lists several articles which treat asymmetric cases of powder patterns with hyperfine and zero-field terms. For example, Mohrmann et al (161) discussed a case of Cr^{3+} in $(NH_4)_2$ [In (H_2O) Cl_5] which has an almost isotropic g-factor ($g_\parallel = 1.987$, $g_\perp = 1.982$) and a completely unsymmetric zero-field splitting ($D = 641G$, $3E/D = 0.25$). Two of the fine structure ($\Delta M_s = \pm 1$) lines produced powder patterns which resembled the one with a completely anisotropic g-factor illustrated in Figure 4. The third or central transition produced a similar pattern with parts of it folded back on itself. This folding back arises from the double valuedness of the maxima in the angularly dependent magnetic field $H(\theta,\phi)$. Measurements at 9.5 GHz and 35.4 GHz and the availability of Hamiltonian parameters from previous single-crystal work helped the authors in their interpretation of the data.

X. SEMIRANDOM DISTRIBUTIONS

The previous three sections treated powder patterns from microcrystallites with randomly oriented axes. The mathematical procedure was illustrated by calculation of the geometric probability factor $G_{(H')}$ for the case of an axially symmetric g-factor.

Sometimes the microcrystallites are not randomly oriented, but have a preferred orientation or distribution $\rho(\delta)$, where δ is the angle between the microcrystallite axis and the preferred direction. The microcrystallites are assumed to be randomly oriented about this preferred axis. For this situation, ESR measurements can be carried out with the magnetic field set at various angles ψ relative to this preferred direction. For each choice of ψ, the spectrum will be an average over microcrystallite distributions, and so will appear powder-like. An analysis of a series of such spectra can provide the distribution function $\rho(\psi)$. More complex distributions in terms of polar angles $\rho(\theta,\phi)$ or Euler angles $\rho(\alpha,\beta,\gamma)$ can also be treated.

Many examples of the magnetic resonance study of semirandom distributions exist (11,187,190-194). For example, McDowell et al (194) reported the ESR spectrum of ClO_2 molecules preferentially oriented in a rare-gas matrix at 4.2% with the molecular plane parallel to the deposition surface. Other paramagnetic species are similarly oriented (195-197). Panepucci and Farach (11) found apatite microcrystallites in irradiated bone to be preferentially aligned along the bone axis. Blazha et al (187) were able to reconstruct the semirandom defect distribution around a paramagnetic center from an analysis of the lineshape. Hentschel et al (198) treated a distribution function $\rho(\alpha,\beta,\gamma)$ expressed in terms of Euler angles α, β, γ and used an expansion of this function in terms of Wigner matrices. They discussed the application of these results to the magnetic resonance of drawn polymers, partially ordered solids, and spin-labeled complexes.

To describe the situation mathematically for a cylindrically symmetric microcrystallite distribution, we select a Cartesian coordinate system with the applied magnetic field in the z direction, the preferred axis ρ for the distribution function in the xz plane with a polar angle ψ, and the crystallite axis c in a general θ,ϕ direction. In this coordinate system, the crystallite distribution function $\rho(\delta)$ depends only on the angle δ between the crystallite direction c and the preferred axis ρ. The angle

δ can be written as a function of θ, ϕ, and ψ through the expression

$$\cos\delta = \cos\theta\cos\psi + \sin\theta\sin\psi\cos\phi \tag{49}$$

If equation (30) is expressed in the form

$$\cos^2\theta = \frac{g_\parallel^2 H_\parallel^2 - g_\perp^2 H'^2}{H'^2(g_\parallel^2 - g_\perp^2)} \tag{50}$$

with the aid of equation (32), then $\cos\delta$ can be written

$$\cos\delta = \frac{(g_\parallel^2 H_\parallel^2 - g_\perp^2 H'^2)^{1/2}\cos\psi + g_\parallel(H'^2 - H_\parallel^2)^{1/2}\sin\psi\cos\phi}{H'(g_\parallel^2 - g_\perp^2)^{1/2}} \tag{51}$$

$$= A(H') + B(H')\cos\phi \tag{52}$$

As a result, $\rho(\delta)$ can be treated as $\rho(H',\phi)$ since ψ is a constant for a given spectrum.

To treat the case of a semirandom distribution of this type, equation (36) can be generalized to the form

Semirandom powder-pattern = lineshape

$$\int_{H_\parallel}^{H_\perp}\int_0^{2\pi} P_{(H')}\, G_{(H')}\, Y\left(\frac{H-H'}{\Delta H}\right) dH'\, \rho(H',\phi)\, d\phi$$

$$= \frac{H_\parallel(g_\parallel^2 - g_\perp^2)^{1/2}}{2} \int_{H_\parallel}^{H_\perp} \frac{(H'^2 + H_\parallel^2)\, Y_{(H')}\, dH'}{(g_\parallel^2 H_\parallel^2 - g_\perp^2 H'^2)^{1/2} H'^2} \int_0^{2\pi} \rho(H',\phi)\, d\phi \tag{53}$$

We should note that the ϕ dependence conveniently factors from the integral. Panepucci and Farach (11) treated the case of an experimental distribution exp ($\alpha\cos\delta$) where α was evaluated from the fit of calculated to experimental spectra.

XI. AMORPHOUS OR GLASSY DISTRIBUTIONS

In sections VII-X, we discussed lineshapes from spin systems with definite Hamiltonian parameters for which the samples consist of microcrystallites with a random or semirandom orientation. These situations occur with an ionic or molecular crystal in which the paramagnetic species has a definite site symmetry. A glassy or amorphous substance is a different kind of material in which a given ion or radical can exhibit a range of Hamiltonian parameters. The powder spectrum of such a material is an average not only over angles but also over Hamiltonian parameters. As a result, different techniques are often applied to calculate the powder spectra of amorphous solids.

A simple example can illustrate how glassy samples produce spectra which differ from those of powders. Consider the case of an axially symmetric g-factor in which the most prominent powder-pattern features appear in resonance absorption at the field value $H = H_\perp$, as indicated in Figure 3. If the paramagnetic species is at a site of axial symmetry with a fixed value of $g_\parallel$ and a range of values of $g_\perp$, then the resonance absorption of the $g_\perp$ points will be spread over a range of field strengths, whereas the absorptions from all of the spins at the $g_\parallel$ point will superimpose and add. As a result, the most prominent feature on the spectrum will correspond to the $g_\parallel$ point. Thus, the basic principle in the interpretation of spectra from glassy samples is the determination of field strengths that correspond to regions of absorption by spins with a range of site symmetries. Such field strengths where many different Hamiltonian values produce a superimposed absorption are referred to as stationary points.

As an example of how the spectra from amorphous samples can be interpreted, consider the case of a ^6S transition ion such as Fe^{3+}, which has the Hamiltonian (199)

$$H = g\beta H\cdot S + D[S_z^2 - 1/3\, S(S+1)] + E(S_x^2 - S_y^2)$$

where g is isotropic, D ranges over values greater than the Zeeman term

$$g\beta H < |D| < D_{max}$$

and the asymmetry parameter $\eta = 3E/D$ can range between 0 and 1

$$0 \le \eta \le 1$$

Since $S = 5/2$ for a ^6S state, there are, in general, six energy levels, and the observed spectrum arises from various transitions between these levels. Energy absorption will occur at those magnetic field strengths H where the distance between two energy levels equals the microwave energy $h\nu$. Associated with such an absorption of energy, we can define an effective g-factor $g = h\nu/\mu_B H$. If we define the magnetic field H_o by setting $h\nu$ equal to $g_o\mu_B H_o$, where g_o is the free electron value, then

$$H_o = h\nu/g_o\mu_B$$

and we can write the following expression for the magnetic field H where resonant absorption occurs

$$H = H_o\left(\frac{g_o}{g}\right) \tag{54}$$

Associated with each value of D and η and with each orientation of the magnetic field at a fixed microwave frequency, there is a series of transitions, each of which is characterized by an effective g-value. After solving the Hamiltonian problem by diagonalizing the matrix associated with H of equation (54), a series of graphs can

be made in which g_o/g is plotted against $D/h\nu$ for a fixed value of η and a particular orientation (199). Figure 6 illustrates such a graph for $\eta = 0.6$, with the individual curves corresponding to the magnetic field aligned along the *x, y,* and *z* principle directions. The most characteristic feature of this graph is the fact that most of the curves are fairly horizontal for values of $D/h\nu$ greater than unity. The g-factors corresponding to such flat regions are called stationary values. As a result of such stationary regions, crystallites with a range of zero-field splittings will absorb microwaves at close to the same magnetic field position. Plots as shown in Figure 6 can be constructed for various values of η and for a series of orientations, and the g-factors where the curves are flat can be compared with experimentally observed g-factors to deduce the range of *D* and *E* values in the sample. Aasa (200) has graphs similar to Figure 6, but plotted g/g_o and $D/h\nu$ on logarithmic scales. Taylor et al (123) have reviewed this field. Table 4 summarizes the results presented in some representative articles.

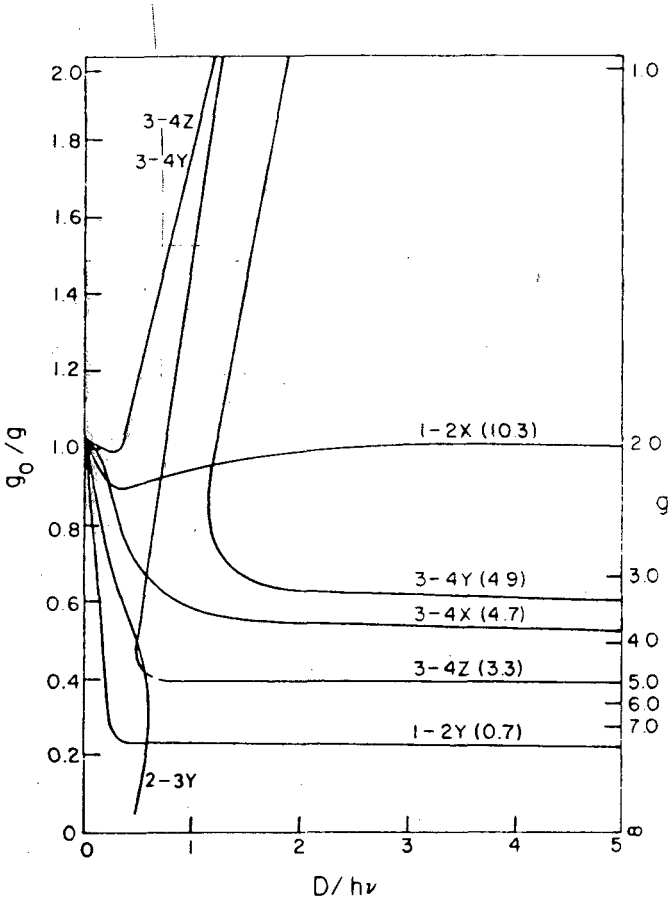

Figure 6. Graph of g_0/g vs $D/h\nu$ for some effective *g* values (given on righthand ordinate axis). Labels on curves indicate the transition, magnetic field orientation (*x, y,* or *z* principal direction), and the relative transition probability (in parentheses) for the region $3 < D/h\nu > 4$ (from reference 199).

XII. INTERMEDIATE MOTIONS IN SOLUTIONS

We now turn our attention from rigid crystalline or amorphous lattices to fluids in which the rapid molecular motion averages out many of the features that dominate the spectra of solids. High viscosity liquids lie in a transition region where spectral features are intermediate between those of a rigid lattice and those of a fluid. The features vary continuously between the two extremes as the viscosity changes. In this section we will consider the region of intermediate motion.

Theoretical studies involving intermediate motion are available (219-229). Here, we will attempt only to delimit the region of intermediate motion in terms of characteristic times, discuss some of the significant underlying mechanisms, and illustrate lineshape changes.

The Brownian motion of a liquid is characterized by a correlation time τ which is a measure of the rapidity of the motion. In classical dielectric relaxation experiments, the molecules are treated as spheres of radius *a* undergoing isotropic rotational reorientation in a medium of viscosity η, and the resulting Debye correlation time τ_D varies inversely with the temperature in accordance with the Einstein-Stokes relationship

$$\tau_D = \frac{1}{2D} = \frac{4\pi\eta a^3}{kT} \tag{55}$$

where *D* is the rotational diffusion coefficient (111). The corresponding correlation time τ_c for the motion of the magnetic moments in an electron spin resonance experiment is one-third the classical Debye value

$$\tau_D = 3\tau_c \tag{56}$$

corresponding to

$$\tau_c = \frac{1}{6D} = \frac{4\pi\eta a^3}{3kT} \tag{57}$$

which relates explicitly to the isotropic rotational model.

From a more general viewpoint, if we consider τ_c as the correlation time for random perturbations involved in ESR measurements, and τ_D as the corresponding dielectric relaxation counterpart, then

$$\tau_D = f\tau_c \tag{58}$$

where *f* varies between 1 and 3 and assumes the limiting value of 3 for the isotropic Brownian model mentioned above. If the random motion is described by a jump model wherein the molecules reorient via large angular shifts of random length, then $\tau_c = \tau_D$, i.e., $f = 1$.

To understand the significance of the correlation time τ_c, consider the situation wherein a random field $\vec{H}_{(t)}$, which perturbs the motion of a spin at a time *t*, tends to change appreciably in a time *t* of the order of τ_c. This means that for times $t < \tau_c$, the perturbing field will have altered very little from its value at $t = 0$, and for times *t*

Table 4. Selected Reports of Lineshapes in Glasses

Symmetries			Center system	Comments	References
g-factor g	Hyperfine A	Zero-field D			
isotropic	isotropic	averaged	Mn^{2+} borate glass	$3E/D = 0$; basic calculation	201
isotropic	asymmetric	—	irradiated borate glass	complex calculation	202,203
isotropic	—	gives values	Mn^{2+} Fe^{3+} complexes	gives $3E/D$ values, good graphs	200
isotropic	isotropic	range	Mn^{2+} borate glasses	gives $3E/D$ range; computer data fit	204
isotropic	isotropic	$g\beta H$	Mn^{2+} As-Te-I glasses	$3E/D = 1$, discusses $g \simeq 30/7$ line	205
isotropic	—	several	Gd^{3+}	several $3E/D$ values, g_o/g vs $D/h\nu$ graphs	206
isotropic	isotropic	—	electron	good graphs	121,207,208
axial	axial	—	E′ center in silica	computer simulation	209,210
axial		—	Fe^{3+}, Ti^{3+}, various glasses	discusses integration	211-213
isotropic	—	range	Mn^{2+}, Fe^{3+}, alumina	gives $3E/D$ range, g_o/g vs $D/h\nu$ graphs	199
axial	axial	—	Cu^{2+} alkali silicate	determines quadrupole moment	214,215
asymmetric	—	—	Cd^{2+} Na glasses	reviews theory	216
asymmetric	—	—	Mn^{3+} As glasses	structure changes	35,217
axial	axial	—	Cr^{2+}, V^{4+} phosphate	computer-simulated glass ΔH	218

$\gg \tau_c$, the perturbing field will be randomly related to its initial value. The time interval τ_c is the crossover point from appreciable to negligible correlation between the random field $\vec{H}_{(t)}$ and its previous value.

The situation just described may be expressed analytically by an autocorrelation function $\overline{H_{\alpha(t+\tau)} H_{\alpha(t)}}$ which is a time average of one of the components H_x, H_y, or H_z of $\vec{H}_{(t)}$. A commonly used autocorrelation function is

$$\overline{H_{\alpha(t+\tau)} H_{\alpha(t)}} = \overline{H_\alpha{}^2} \exp(-|\tau|/\tau_c) \qquad (59)$$

In this simple case, the spin-lattice and spin-spin relaxation times T_1, and T_2, respectively, are given by

$$\frac{1}{T_1} = \gamma^2[\overline{H_x^2} + \overline{H_y^2}]\frac{\tau_c}{1+\omega_o{}^2\tau_c{}^2} \qquad (60)$$

$$\frac{1}{T_2} = \gamma^2[\overline{H}_z{}^2\tau_c + \tfrac{1}{2}(\overline{H}_x{}^2 + \overline{H}_y{}^2)\frac{\tau_c}{1+\omega_o{}^2\tau_c{}^2}] \qquad (61)$$

which gives for the linewidth

$$\Delta\omega_{1/2} = \gamma\Delta H_{1/2} = \frac{2}{T_2} \qquad (62)$$

The perturbing fields generally are isotropic, $\overline{H}_x{}^2 = \overline{H}_y{}^2 = \overline{H}_z{}^2$, which gives

$$T_1 = T_2 \qquad \omega_o\tau_c \ll 1 \qquad (63)$$

$$T_1 \gg T_2 \qquad \omega_o\tau_c \gg 1$$

the former being typical of low-viscosity liquids and the latter of solids.

The discussion thus far has concerned a single symmetrical resonant line having a width that varies in accordance with the factor $\omega_o\tau_c$. Of greater interest is the effect on powder-pattern spectra arising from asymmetric Hamiltonian tensors. In this case, the critical parameter is the ratio $2\tau_c/T_2$ which equals $\tau_c\Delta\omega_{1/2}$ by substitution from equation (62).

In the slow motion regime corresponding to $\tau_c\Delta\omega_{1/2} \gg 1$, a rigid lattice powder pattern is obtained, while at the rapid motion limit $\tau_c\Delta\omega_{1/2} \ll 1$, the powder pattern collapses to a singlet characteristic of a liquid. At intermediate rates of reorientation, where $\tau_c\Delta\omega_{1/2} \simeq 1$, the lineshape is a poorly resolved or partially collapsed powder pattern.

Sillescu (230) examined these various cases in terms of a fluctuating time-dependent axially symmetric Zeeman Hamiltonian

$$H_{(t)} = \mu_B[g_\perp(S_xH_x + S_yH_y) + g_\parallel S_zH_z] \qquad (64)$$

If one adopts the notation

$$g_o = \frac{1}{3}(g_\parallel + 2g_\perp) \qquad (65)$$

$$\Delta g = (g_\parallel - g_\perp) \qquad (66)$$

then in the limit of $|\Delta g| \ll g_o$ the Hamiltonian becomes

$$H_{(t)} = g_o\mu_B HS_z + \frac{1}{3}\Delta g(\cos^2\theta(t) - 1)\mu_B HS_z \qquad (67)$$

where the time dependence arises from random local fluctuations in the angle $\theta(t)$ with the correlation time τ_c. If $\tau_c\Delta\omega_{1/2}$ greatly exceeds unity, then very little averaging occurs and the observed spectrum is a powder pattern of the type illustrated in Figures 3 and 7. In the opposite limit, when $\tau_c\Delta\omega_{1/2}$ is much less than unity, then the factor

$3\cos^2\theta(t) - 1$ is almost averaged out to produce the slightly asymmetric singlet illustrated in Figure 8. The intermediate case, where $\tau_c\Delta\omega_{1/2} \simeq 1$, corresponds to a partially averaged but still recognizable powder pattern as presented in Figure 9. The presentation of curves for both the rotational Brownian motion and random-jump models shows the effect of random fluctuation on lineshape. We see that for the same value of $\tau_c\Delta\omega_{1/2}$, the Brownian motion model leaves the powder-pattern features somewhat more prominent than in the random-jump model.

In the slow motion region, i.e., τ_c between about 10^{-9} and 10^{-6}s, partially averaged powder-pattern spectra are observed. For shorter times, τ_c becomes of the order of the period of microwaves ($\omega_o\tau_c \simeq 1$), and for even shorter times, $\omega_o\tau_c \ll 1$. For longer correlation times, $\tau_c > 10^{-6}$s, the rigid lattice limit is approached. Various authors (228,231-234) have treated the completely anisotropic and axially symmetric g-factor lineshapes at intermediate correlation times, and some (235-240) included hyperfine interactions (see Table 5).

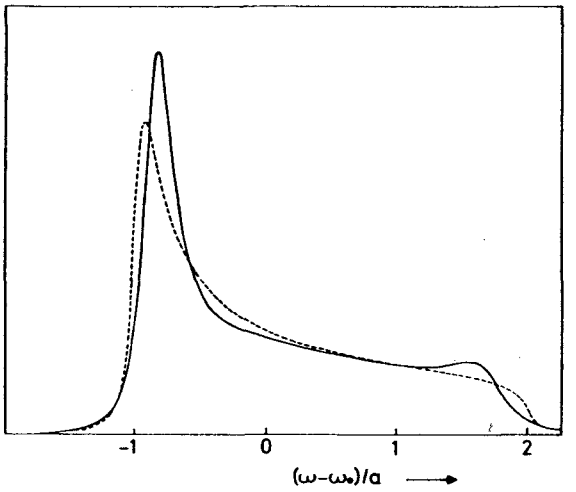

Figure 7. ESR spectrum in the slow-reorientation region $\tau\Delta\omega_{1/2} = 200$ arising from a slightly averaged, fluctuating, axially symmetric Zeeman Hamiltonian–Brownian-motion model--jump model (from reference 230).

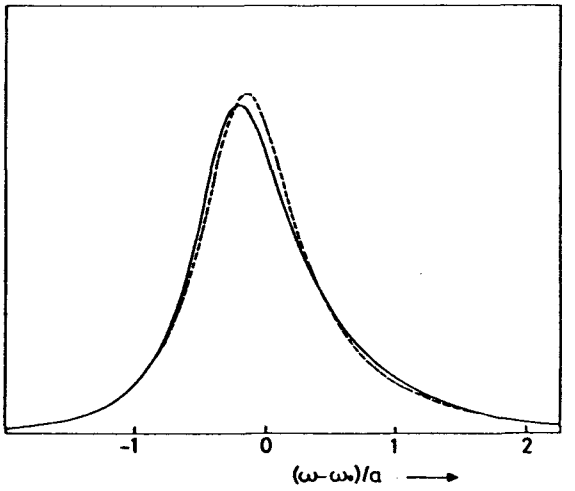

Figure 8. ESR spectrum in the rapid-reorientation region $\tau\Delta\omega_{1/2} = 0.6$ arising from an almost completely averaged, fluctuating, axially symmetric Zeeman Hamiltonian–Brownian-motion model--jump model (from reference 230).

XIII. HINDERED ROTATIONS AND TUNNELING

Hindered rotation or tunneling motions can influence the number, position, and widths of the lines in a hyperfine multiplet. For example, a hindered methyl group undergoing tunneling rotation at liquid-helium temperature produces an eight-line spectrum, while the same methyl group freely rotating at high temperatures produces a 1:3:3:1 intensity ratio quartet (246-248). In an argon matrix at 4.2 K, the α and β proton hyperfine tensors of the ethyl radical are axially symmetric due to rapid reorientation about the C-C bond (249), and *n*-propyl and *n*-butyl radicals exhibit motional or tunneling effects (250). Maruani et al (251) published axial hyperfine couplings for the CF_3 radical, and Vugman et al (252) reported axial rotation of H_2CN.

Freed (253) analyzed the effects of internal motions of methyl groups on hyperfine patterns, taking tunneling into account. His results agree with classical theory when the hyperfine frequency exceeds the tunneling rate, while quantum effects become important under the opposite condition.

When two or more isotropic hyperfine coupling constants are modulated by fluctuating fields at rates that are comparable to their difference expressed in frequency units, then the spectra exhibit selective

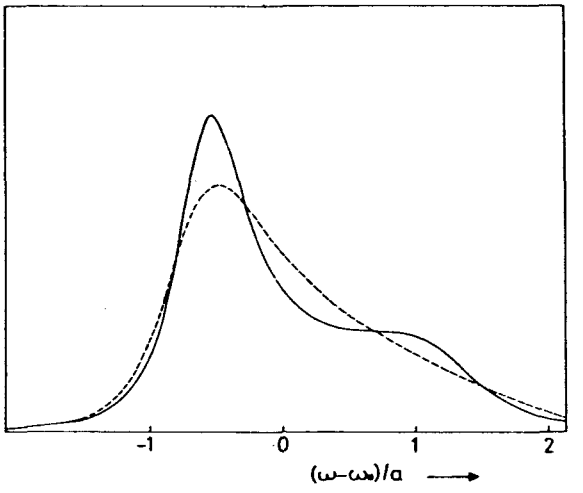

Figure 9. ESR spectrum in the intermediate-reorientation region, $\tau\Delta\omega_{1/2} = 4$ arising from a partially averaged, fluctuating, axially symmetric Zeeman Hamiltonian–Brownian-motion model--jump model (from reference 230).

Table 5. Lineshapes of Intermediate and Slow Motion Systems
(See Table 11 for spin-label data.)

Symmetries		τ_c, s	Model	Comments	References
g-factor *g*	Hyperfine *A*				
—	—	wide range	—	spin pairs	241
axial	—	$0.3<\tau_c\Delta\omega<10^2$	isotropic rotational diffusion	Markov process	228
asymmetric	axial	$0.07<\tau_c\Delta\omega<70$	rotational diffusion	imino acid radicals, H_2O glycerol	237
isotropic	axial	—	Brownian motion	rotating methyls	167,168
asymmetric, axial	asymmetric, axial	10^{-9} to 10^{-6}	Brownian, jump, isotropic, and anisotropic diffusion	peroxylamine disulfonate (PADS), τ_c estimated	239
asymmetric	axial	$1.3<\tau_c\Delta\omega<6.6$	rotational diffusion	—	236
asymmetric, axial	axial	wide range	isotropic rotational diffusion	Monte Carlo	240
isotropic	isotropic, axial	3×10^{-12} to 10^{-6}	Brownian, rotational, jump, isotropic, and anisotropic	peroxylamine disulfonate (PADS) in glycerol-H_2O	242,243
axial	—	2×10^{-10} to 4×10^{-8}	Brownian, jump	sulfur in 60% oleum	233
asymmetric	asymmetric	wide range	jump	partially ordered powder	235,238
axial	—	$4<\tau_c\Delta\omega<10^4$		continued fractions, axially symmetric zero-field *D*	244,245
axial	—	wide range	axial diffusion	projection operators	231
axial	—	wide range	—	graphical techniques	232

broadening. Krusic et al (254) discussed the case wherein hindered rotation caused such modulation via twofold potential barriers. They present data on the CH_2OH radical in which the α protons are equivalent at 215 K and nonequivalent at 148 K. At intermediate temperatures such as 183 K, tunneling broadens the lines.

When frozen in place at low temperatures, the CO_2^- radical ion in calcite has three equilibrium configurations corresponding to three ways in which the two oxygens of CO_2^- can occupy the three CO_3^{2-} oxygen sites, and each gives a separate spectrum (15). At high temperatures, free rotation causes the three lines to coalesce into one. At intermediate temperatures, where the tunneling jump rate is comparable to the Zeeman frequency $g\mu_B H/\hbar$, the spectrum is broad and poorly resolved. The calculated angular dependence of the linewidth in the intermediate temperature region agreed qualitatively with experimental results.

Krishnamurthy (23) found that the vanadyl (VO^{2+}) ion in $VO_2(NO_3)_2 6H_2O$ undergoes a rapid reorientation or hindered motion at room temperature which produces a solution-like spectrum. At low temperatures, the vanadyl ion freezes in place with a random orientation and displays a powder-pattern spectrum.

Raoux (255) explained the ESR spectrum of an H center in irradiated LiF in terms of the rotation of the molecule about the average (111) direction induced by librations and pyramidal jumping between the four (111) directions. The inhomogeneous Gaussian line recorded at low temperature broadens above 150 K due to a homogeneous Lorentzian contribution from reorientational effects.

Chase (256) examined the resonance from Eu^{2+} in alkaline earth fluorides and found a tunneling energy level about 5 cm^{-1} above the ground level. He calculated lineshapes for the competition between strain and tunneling effects associated with a dynamical Jahn Teller distortion.

Table 6 summarizes representative data on hindered rotation and tunneling effects.

XIV. CONCENTRATION AND TEMPERATURE DEPENDENCE

Free radicals and transition ions in solution or in rigid solids have linewidths which tend to increase linearly with concentration from a residual value at zero concentration, in accordance with the expression

Table 6. Effect of Hindered Rotation and Tunneling on Lineshapes

System	Group	Temperature, K	Comments	Reference
n-propyl, n-butyl	CH_2	4.2	axial Hamiltonian	250
CH_3OH radical	CH_2	120 to 330	theoretical explanation	254
$C_2H_4 + H_2$	CH_2CH_3	4.2	axial Hamiltonian	249
theoretical	CH_3	wide	theory, spin-rotation coupling and rotational relaxation	253
CH_3CH_2 radical	CH_3	4.2 to 80	explanation	247
L-alanine	CH_3	4.2 to 80	explains temperature dependence	248
azobisisobutyronitrile	CH_3		computer simulation	167,168
CF_2CONH_2	C-C	77 to 290	torsional motion	17
$CH_3\dot{C}OHCOO^-$	CH_3	2 to 20	weakly hindered	246
$R\dot{C}CH_3$ radical	CH_3	4.2	ENDOR	257
p-x-acetophenone	acetyl	241 to 322	hindered rotation activation energy	258
calcite $CaCO_3$	CO_2^-	400 to 500	theoretical explanation	15,259
$[Ni(NH_3)_6](BF_4)_2$, related compounds	NH_3	80 to 330	ordering temperature found	260
dinitrophenyl, dinitronaphthalene	NO_2	193 to 293	seesaw motion	261
AsO_4^{4-}	H bond tunn.	wide	jump theory	235,238
Na, SO_2, O_2	$NaSO_2$, NaO_2	4.2	Ar matrix	262
$(GeO_x^-)^-$	$xSiO_2$	15 to 300	3 orientations, jumping	263
LiF	H center	77 to 220	libration	255
$UO_2(NO_3)_26H_2O$	VO_2	120 to 300		23
Cs_2HfCl_6, Cs_2ZrCl_6	Mn^{2+}	12 to 400	3-site axis jump	264
$Cu(en)_3^{2+}$	$Cu(en)_3^{3+}$	77	pulse radiolysis	265
CaF_2	Eu^{2+}	1.5 to 4	Jahn Teller	256

$$\Delta H = \Delta H_0(1 + aC) \qquad (68)$$

where C is the concentration and a is a constant. The factor ΔH_0 arises primarily from dipolar interactions.

When the concentration becomes large enough, exchange effects become appreciable, and at high concentrations the exchange interaction causes the lines to narrow. The quantities ΔH_0 and ΔH_1 are strongly temperature dependent in solutions due to the motional narrowing influence of Brownian motion, and are less temperature dependent in solids which lack Brownian fluctuations. There are exceptions to this rule, attributable to such mechanisms in solids as internal molecular rotations and tunneling.

To illustrate the manner in which the factors in equation (68) depend on temperature, we will summarize the results of a study by Ayant and coworkers (266,267) of the deuterated tanone radical (tetramethyl 2,2,6,6, piperidone – 4, oxide) which gives a triplet hyperfine pattern due to the nuclear spin $I = 1$ of the nitrogen. Both ΔH_0 and ΔH_1 of equation (68) depend on η/T, the ratio of viscosity to temperature, through the correlation time τ_c for which the Debye approximation is given in equation (56). Ayant showed that the concentration-independent width ΔH_0 has the relationship

$$\Delta H_0 = a\frac{T}{\eta} + b + (A + BM + CM^2)\frac{\eta}{T} \qquad (69)$$

The first term, aT/η, comes from the spin-rotational interaction; b is due to unresolved hyperfine interactions and instrumental effects; and the third set of terms is related through M to the hyperfine component line (to be discussed in section XV). The concentration-dependent width ΔH_1 of equation (68) has the relationship

$$\Delta H_1 = d\frac{\eta}{T} + e\frac{T}{\eta}\phi(T/\eta) \qquad (70)$$

which has a dipolar part $d\eta/T$ and an exchange part which depends on temperature through the complex function $\phi(T/\eta)$. Calculations agreed satisfactorily with

Table 7. Concentration Dependence of Linewidths

System	State	ΔH-vs-concentration graph	Comment	References
radical $S = ½$, metal ion $S > ½$	solution		mutual linear concentration broadening	61,62
$ON(SO_3)_2^{2-}$	aqueous	yes	measured relaxation	271
several radicals	THF, DGDE	yes	250 to 310 K	272
piperidine radicals	H_2O, glycerol	yes	broadening by transitions	67,268
tanon	methanol	yes	183 to 363 K	266,267
Cr^{3+}, Fe^{3+}	H_2O glycerol	yes	H_2O/glycerol ratio varied; X and Q bands	273
$[Fe(H_2O)_nF_{6-n}]^{3-n}$	aqueous	—	complexes $n=0$ to 6	274
$Mn(C10_4)_2$	methanol, DMF, DMSO, CH_3CN, acetonitrile	yes	O_h and tetrahedral complexes	275,276
$Mn(NO_3)_2$	solution, H_2O	yes	290 to 370 K	277
$Mn(NO_3)_2$	H_2O	no	200 to 360 K	278
$MnCl_2$-KCl	liquid	yes	total concentration range studied	279
ion implantation	layer	yes	effective donor concentration varied	280
9,10 dimethyl-anthracene	silica alumina surface	no	surface site dependence	281
butadiene radicals	silica gel surface	no	hfs concentration dependence	282
irradiated NaOH	aqueous glass	yes	H_2O/D_2O ratio plot	208
N in diamond	single crystal	no	N-N interaction	283
diamond	solid	yes	temperature dependence	284
n-type In Sb	solid	yes	theoretical explanation	285
CdS	single crystal	yes	donor concentration studied	286
Si-Ge alloy	amorphous	yes	ΔH increases with Ge/Si ratio	287,288
V^{4+}/VOPO	glass	yes	antiferromagnetic coupling	289
Cr^{3+}	single crystal	yes	Cr^{3+}-Li^+ pairs give angle-dependent ΔH	31
$Cr^{3+}/(Cr,Al)_2O_3$	powder	yes	total concentration range	269,270
Cr^{3+} alum	—			32
Cr^{3+}/Al_2O_3	single crystal	yes	optically detected ^2E state	290
$Mn(CH_3COO)_24H_2O$	single crystal	no	ΔH angle- and temperature dependent	291
$Mn^2/Mg(HCOO)_22H_2O$	single crystal	yes	2-dimensional magnetic lattice	36
MnO-MgO and NiO-MgO	solid	no	MnO Lorentzian, NiO Gaussian	292
$Cu(en)_3^{2+}$	glass	yes	e-tunneling	265
$Gd(Co_xNi_{1-x})_2$	polycrystalline	no	temperature dependence	293
Gd^{2+}/La and $LaAl_2$	solid	yes	bottleneck relaxation	294
Dy/$GdAl_2$	solid	yes	temperature dependence	295

experiment from 183 K to 363 K for concentrations from 0.2×10^{-3} to 4×10^{-3} mol l^{-1}. Anisimov et al (268) found that equation (70) was satisfied by two piperidine-type radicals when lines were broadened by the paramagnetic nitrates of iron-group transition ions, with cadmium nitrate used as a blank to eliminate nonparamagnetic effects.

Concentration-dependent effects are also important in solids. For example, the narrow lines arising from Cr^{3+} ions in ruby (Al_2O_3) broaden with increasing chromium content, and then begin to narrow again for large Cr/Al ratios (269,270). Tables 7 and 8 list results of studies of concentration and temperature dependence in solutions and solids.

Pressure dependence has also been studied, for example, by Filippov and Donskaya (335,336) on VO^{2+}, Cr^{3+}, and Mn^{2+} in aqueous solutions up to 6000 atm. Grouchulski et al (324) studied temperature dependence in MnTe at 1, 2, and 4 kbar.

Continued on p. 184

Table 8. Linewidth Temperature Dependence in Liquids and Solids

System	State or solvent	ΔH-vs-temperature graph	Temperature, K	Comments	References
(p-x-acetophenone)$^+$ x=NO_2, CH_3, H, Br, and OCH_3	DMF	vs $1/T$	241-322	acetyl hindered rotation	258
benzene anion, tropenyl	THF, DME	vs η/T	150-275	CW saturation	297
$C10_2$	TBP	vs T/η	variable	^{35}Cl HFS	298
dinitro radicals	DMF	no	193-293	out-of-phase correlation	261
DPPH	toluene	no	232-314	spectra vs temperature	299
amino acid radicals	glycerol	—	200-291	rotational diffusion, anisotropic interaction	237
semiquinones	ethanol, butanol	vs η/T	77-300	tumbling studied	300
tanone	isopropanol and others	no	140-300	transition from normal to supercooled liquid	301-303
several radicals	THF, DGDE	vs $1/T$	250-310	relaxation	272
$Ti(H_2O)_6^{3+}$	aqueous acid	vs η/T	230-290	plot linear through glass formation	304
Cr, Mo, W dibenzyl iodide	ethanol	no	133-293	spectra vs temperature	305
$MnCl_2$-KCl	self	vs η/T	775-1275	dipolar and exchange	279
$Mn(ClO_4)_2$	ethanol, DMF, DMSO, CH_3CN	yes	250-375	O_h and tetrahedral complexes	276,306
$Mn(NO_3)_2$	H_2O,H_2O-glycerol, H_2O-sugar	—	—	—	278
$Mn(ClO_4)_2$	DMG,DEF,DMSO	vs $1/T$	295-430	fine-structure dependence	162
Mn^{2+}, Fe^{3+}	DMF, TBP, methanol, ethanol	vs $1/T$	180-370	fine-structure dependence	307
$K_3Mo(CN)_8$, $K_3W(CN)_8$	methanol, ethanol	vs $1/T$	180-360	^{14}N SHFS, X and Q bands	308
Eu^{2+}/AgCl	single crystal	yes	93-300	activation energy determined, bleaching studied	309
B	amorphous, single crystal	yes	1.5-1000	activation energy, hopping frequency	310
As-doped Ge	solid	yes	1.5-4.2	concentration dependence studied	288
blue d'outre-mer	solid	yes	77-525	ΔH increases with temperature	311
BrO_3^{2-}/$KBrO_3$	single crystal	yes	26-250	jump model	18
butadiene radical	silica gel surface	no	77-195	irradiation, 3 radical types	282
O_2/N_2	solid	no	1-20	—	177
$CO_3^-/CaCO_3$	single crystal	yes	77-400	3-site hopping	259
ClF_6, BrF_6, IF_6/SF_6	solid	no	27-200	2 sites with different ΔH	312
Ge	amorphous	yes	4-300	O_2, annealing studied	313,314
H center/Li	single crystal	yes	7-150	reorientation motion broadening above 150 K	255
n-type InSb	solid	yes	1.5-40	experiment and theory	285

Table 8. Linewidth Temperature Dependence in Liquids and Solids *(Continued)*

System	State or solvent	ΔH-vs-temperature graph	Temperature, K	Comments	References
donors/CdS	single crystal	yes	1.4-4.2	hopping frequency calculated	286
S film	amorphous	yes	300-1300	annealing studied	313
P-doped Si	single crystal	yes	20-300	localized and delocalized electrons	315
vinyl	silica gel	no	77-300	reversible changes	316
V_2MoO_3	single crystal	yes	4-300	ΔH angle-dependent, e-hopping	317
Cr_2O_3	polycrystalline	yes	290-525	1% and 6% Ga	24
$CrBr_3$	single crystal	yes	20-550	ferromagnetic, T_N = 32.5 K	318,319
Cr^{3+}/GASH	single crystal	no	1.6-300		320
(Cd, Zn, Hg)Cr_2 Se, S)$_4$	single crystal, polycrystalline	yes	100-300	$T > T_N$, relaxation discussed	321
Mn^{2+}/MgTe	single crystal	no	4,77,300		322
Mn^{2+}/TlN_3	single crystal	yes	253-353	ΔH decreases as temperature increases	323
$Mn(CH_3COO)_2 \cdot 4H_2O$	single crystal	yes	77-373	ΔH angular dependence	291
Mn^{2+}/$Mg(HCOO)_2 2H_2O$	single crystal	yes	77,178,298	2-dimensional system	36
MnTe	polycrystalline	yes	300-360	1—4.3 kbar	324
MnO, MnS, MnF_2, $KMnF_3$, $RbMnF_3$, $CsMnF_3$	solid, liquid	yes	300-1500	measured through melting point	325
Fe^+, Fe^{3+}, Mn^{2+}/MgO	single crystal	yes	4.2-300	ΔH dipolar at low temperature, relaxation-limited at high temperature	326
Fe^+/voltaite	powder	yes	1.6-293	measured above 0.7 K ferromagnetic transition	327
Fe^0, Fe^+/Si	single crystal	yes	90-170	$Fe^o \rightarrow Fe^+$ transition at high temperature	328
F^+, Fe^{3+}, Mn^{2+}/MgO	single crystal	yes	4.2-300	relaxation narrowing	326
$NiSiF_6 \cdot 6H_2O$	solid	yes	—	uniaxial anisotropy	88,89
$Cu(HCOO)_2 \cdot 4H_2O$	single crystal	yes	4-260	ΔH angular dependence, e-hopping	24,90,329
Zn/Cu acetate	single crystal	yes	20-120	Lorentzian above 50 K, Gaussian with Lorentzian tails below 40 K	330
Ce, Nd, Sm in LaMg nitrate	single crystal	yes	2-26	T_1/T_2 measured	331
$Gd(Co_xNi_{1-x})_2$	polycrystalline	yes	100-300	concentration dependence studied	293
GdNi, $GdNi_3$, $GdNi_5$	solid	yes	77-700	$\Delta H = a + bT$, localized moments	332
$GdFe_3$	film	yes	4-550	ΔH frequency dependent 8.4-35 GHz	333
Gd in Y	single crystal	yes	3-20	ΔH angle dependent	45
(Gd, Dy)Al_2	solid	yes	150-205	ΔH depends on Gd/Dy ratio	295
Ho^{3+}	single crystal	yes	1.2-25	T_1 measured	56

Table 9. Systems with Hyperfine Component Widths $\Delta H = A + BM + CM^2 + DM^3$

Paramagnetic species	Solvent or matrix	Comments	References
anthracene, perylene, tetracene	silica alumina surface	antisotropic rotation	281
p-benzoquinone anion	H_2O, ethanol, DMSO	—	340
CF_3CONH_2	trifluoracetamide SC	irradiation	17
dichloro acetamide	irradiated single crystal	broader upfield lines	342
di-t-butyl nitroxide	supercooled H_2O	computer simulation	343,344
nitroxide	solution	180—380 K, ^{14}N, ^{15}N	345,346
nitroxide	solution	nematic-isotropic phases	347
peroxylamine disulfonate	glycerol-H_2O	^{17}O doped, theory	242,243
VO_2^+	aqueous solution	X, K bands	337
VO_2^+	alkali halides	ΔH decreases as temperature increases	348
VO_2^{2+} acetylacetonate	various solutions	secular, nonsecular, residual	220,229,349
VO_2^{2+} diketonate	several inert solvents	η/T plots	339
VO_2^{2+} octaethylporphyrin	glass, 100 K	ΔH inversion	350
Cu^{2+}, c-asparagin	aqueous	powder, glass, solution	351
$Cu(ClO_4)_2$	aqueous and methanol	NMR relaxation	352
$Cu(NO_3)_2$	liquid ammonia	195-300 K	353
$Nb(C_5H_5)_4$	toluene	solution and frozen, η/T plots	354
(dihydroxydurene)$^+$	solution	alternating widths	355
(dinitrodurene)$^-$, dinitromesitylene	solution	alternating widths	356
(m-dinitrobenzene)$^-$	solution	alternating widths	357
hydropyrene	DMG, THF, MTHF, H_2SO_4	alternating widths	358-360
pyrazine-alkali	THF, MTHF	triple ions	361,362

XV. HYPERFINE COMPONENT DEPENDENCE

Hyperfine multiplets from radicals or transition ions in solution often exhibit a linewidth that varies with the magnetic nuclear spin quantum number M from one component to the next across the spectrum. Rogers and Pake (337) recorded the hyperfine structure of the vanadyl ion VO_2^{2+} at 9.25 and 24.3 GHz and found that the component dependence of the width was also a function of frequency. Kivelson and co-workers (220-222,229) explained this in terms of incomplete averaging of g-factor and hyperfine coupling anisotropies and derived the formula

$$\Delta H_{1/2} = \Delta H_0 + A + BM + CM^2 \qquad (71)$$

where the linewidth ΔH is related to the spin relaxation time T_2, through a rearrangement of equation (62), by

$$\Delta H_{1/2} = \frac{2}{\gamma T_2}$$

and ΔH_0 is the residual linewidth which often comes from spin-rotational interactions. In the limit of rapid tumbling in strong magnetic fields (e.g. 10^3 or 10^4 gauss), the terms A, B, and C are given by (111)

$$A = \frac{2}{15}(\Delta g)^2\left(\frac{\mu_B H}{h}\right)^2\tau_c + \frac{1}{20}(\Delta a)^2 I(I+1)\tau_c \qquad (72)$$

$$B = -\frac{4}{15}\left(\frac{\mu_B H}{h}\right)(\Delta g \Delta a)\tau_c \qquad (73)$$

$$C = \frac{1}{12}(\Delta a)^2\tau_c \qquad (74)$$

where the factors containing Δg and Δa arise from the deviations of the g-factor and hyperfine tensors from their respective isotropic parts g_o and a_o

$$(\Delta a)^2 = (a_{xx} - a_o)^2 + (a_{yy} - a_o)^2 + (a_{zz} - a_o)^2 \qquad (75)$$

$$(\Delta g \Delta a)^2 = (a_{xx} - a_o)(a_{xx} - g_o) + (a_{yy} - a_o)(g_{yy} - g_o) + (a_{zz} - a_o)(g_{zz} - g_o) \qquad (76)$$

Other interactions can also contribute to A, B, and C.

The factor $(\mu_B H_o/h)$ causes the widths to depend on the frequency band. The term BM gives the spectrum an unsymmetric appearance. A more refined theory adds

the terms EM^3 and FM^4 to equation (71), but these are usually small. For rotational diffusion in the Debye approximation, τ_c is given by equation (57).

Wilson and Kivelson (229) sorted out the secular and nonsecular contributions to *A, B, C,* and *D* and obtained the residual linewidth ΔH_o by subtracting calculated values of *A* from measured values of $A + \Delta H_o$. For vanadyl acetylacetonate, ΔH_o came from spin-rotational relaxation and was proportional to T/η. Residual linewidths in solutions commonly derive from the spin-rotation interaction (338). Eagles and McClung (339) studied vanadyl β diketonate complexes and found deviations from the Kivelson linewidth theory at low temperatures and high viscosities.

Equations (71) through (76) were derived for the high fields typical of X-band (3400 gauss, 10^4 MHz) spectra. Barbarin and Germain (340) derived analogous expressions for low fields (30 gauss, 80 MHz) and carried out measurements at both high- and low-frequency bands to evaluate the contribution to the linewidth from the g-factor and hyperfine anisotropies.

Bogomolova et al (218) analyzed the powder spectra of Cu and V glasses with the aid of the expressions

$$\begin{aligned} \Delta H_{\parallel}^2 &= A_{\parallel} + B_{\parallel}M + C_{\parallel}M^2 \\ \Delta H_{\perp}^2 &= A_{\perp} + B_{\perp}M + C_{\perp}M^2 \\ \Delta H^2 &= \Delta H_{\parallel}^2 \cos^2\theta + \Delta H_{\perp}^2 \sin^2\theta \end{aligned} \tag{77}$$

Freed et al (341) used a stochastic Liouville approach to the theory of the hyperfine component dependence of the linewidth.

Table 9 summarizes other recent work on this dependence.

XVI. ALTERNATING LINEWIDTHS

Freed and Fraenkel (363) considered linewidths from hyperfine patterns in which nuclei are symmetrically but not completely equivalent. This means that the nuclei are equivalent with respect to the zero-order Hamiltonian so that they have the same gyromagnetic ratios ($\gamma_i = \gamma_j$), spins ($I_i = I_j$), and hyperfine interaction constants ($A_i = A_j$), but are not equivalent with respect to a perturbing Hamiltonian such as the dipolar interaction ($H_{ddi} \neq H_{ddj}$). Completely equivalent nuclei also have the same perturbing Hamiltonian ($H_{ddi} = H_{ddj}$). The particular case studied concerned two nuclei with widths that vary as CM^2 when the nuclei are completely equivalent, i.e.,

$$\Delta H_{1/2} = CM^2 \tag{78}$$

where

$$M = M_1 + M_2 \tag{79}$$

and

$$|M| \leq 2I \tag{80}$$

If the two nuclei are incompletely equivalent, then the width of a hyperfine line with $M = M_1 + M_2$ depends on the magnetic quantum numbers as follows

$$\begin{aligned} \Delta H_{1/2} &= \sum_{i,j} j_{ij} M_i M_j \\ &= j_{11} M_1^2 + j_{22} M_2^2 + (j_{12} + j_{21}) M_1 M_2 \end{aligned} \tag{81}$$

Since $j_{11} = j_{22}$ and $j_{12} = j_{21}$, this becomes

$$\Delta H_{1/2} = j_{11} M^2 + 2(j_{12} - j_{11}) M_1 M_2 \tag{82}$$

Each hyperfine line has a degeneracy of 1 if $M_1 = M_2$ and 2 if $M_1 \neq M_2$, since in the latter case (M_1, M_2) and (M_2, M_1) give superimposed lines.

Table 10 presents the results for $\Delta H_{1/2}$ obtained with the nuclei $I = 1/2$, 1, and 3/2. The last three columns of the table give the values for the in-phase case ($j_{12} = j_{11}$), where the nuclei are completely equivalent and equation (82) reduces to equation (78), the out-of-phase case ($j_{12} = -j_{11}$), and the uncorrelated case ($j_{12} = 0$), which have the respective widths

$$\Delta H_{1/2} = \begin{cases} j_{11}(M_1 + M_2)^2 & j_{12} = j_{11} \text{ in phase} \\ j_{11}(M_1 - M_2)^2 & j_{12} = -j_{11} \text{ out of phase} \\ j_{11}(M_1^2 + M_2^2) & j_{12} = 0 \text{ uncorrelated} \end{cases} \tag{83}$$

The general case produces linewidths which vary in a complex manner from one hyperfine component to another. For some choices of the ratio j_{12}/j_{11}, certain hyperfine components have very narrow widths and others are broad. The theory explains some observed spectra in which the widths of successive components tend to alternate between wide and narrow, and other observed spectra in which the component amplitudes deviate from the binomial case due to the broadening of some components beyond detection. For example, in the out-of-phase case with $I_1 = I_2 = 1$, if j_{11} is very large, the $M = \pm 1$ lines will be broadened beyond detection and the hyperfine pattern will appear as an equal intensity triplet arising from the M = 0, ± 2 lines, rather than as a 1,2,3,2,1 quintet. This phenomenon has been observed experimentally (363).

Goldman et al (242) fitted the linewidth data of ^{17}O-labeled peroxylamine disulfonate in glycerol water mixtures to the expression

Table 10. Secular Linewidths, Isotropic Modulation of Two Nuclei (from reference 363)

I	M	(m_1,m_2)	D_k	General	$[T_{2,k}^{(m)}(\text{sec})]^{-1}$ In-phase correlated $j_{12}=j_{11}$	Out-of-phase correlated $j_{12}=-j_{11}$	Uncorrelated $j_{12}=0$
½	±1	(±½, ±½)	1	½($j_{11}+j_{12}$)	j_{11}	0	½j_{11}
	0	[±½, ∓½]*	2	½($j_{11}-j_{12}$)	0	j_{11}	½j_{11}
1	±2	(±1, ±1)	1	2($j_{11}+j_{12}$)	$4j_{11}$	0	$2j_{11}$
	±1	[±1, 0]	2	j_{11}	j_{11}	j_{11}	j_{11}
	0	(±1, ∓1)	2	2($j_{11}-j_{12}$)	0	$4j_{11}$	$2j_{11}$
		(0, 0)	1	0	0	0	0
3/2	±3	±3/2, ±3/2	1	9/2($j_{11}+j_{12}$)	$9j_{11}$	0	9/2j_{11}
	±2	[±3/2, ±½]	2	½(5$j_{11}+3j_{12}$)	$4j_{11}$	j_{11}	5/2j_{11}
	±1	[±3/2, ∓½]	2	½(5$j_{11}-3j_{12}$)	j_{11}	$4j_{11}$	5/2j_{11}
		±½, ±½	1	½($j_{11}+j_{12}$)	j_{11}	0	½j_{11}
	0	[±3/2, ∓3/2]	2	9/2($j_{11}-j_{12}$)	0	$9j_{11}$	9/2j_{11}
		[±½, ∓½]	2	½($j_{11}-j_{12}$)	0	j_{11}	½j_{11}

*Square brackets indicate inclusion of both (m_1, m_2) and (m_2,m_1) states.

$$\Delta H_{½} = A_N + A_O + B_N M_N + B_O M_O + C_N M_N^2 + C_O M_O^2 + D M_N M_O \quad (84)$$

where the subscript N refers to the nitrogen nuclei (I_N = 1) and O denotes ^{17}O (I_O = 5/2). The constant A_N is the width of the central line (M_N = 0) in the undoped radical. The various factors were determined at 5, 13, and 21°C. High power studies indicate that the three hyperfine lines of the undoped radical saturate at different power levels, the central component saturating first. Table 9 lists articles which discuss alternating linewidths.

XVII. FINE STRUCTURE EFFECTS

The linewidth within a fine structure multiplet can also vary with the particular fine structure transition $|M_s\rangle \leftrightarrow |M_s \pm 1\rangle$ due to modulation of the zero-field Hamiltonian term $\vec{S}\cdot\overleftrightarrow{D}\cdot\vec{S}$. Using the notation

$$\begin{aligned} d_{xx} &= -\frac{1}{3}D + E \\ d_{yy} &= -\frac{1}{3}D - E \\ d_{zz} &= \frac{2}{3}D \end{aligned} \quad (85)$$

we can write for the inner product of the traceless $\overleftrightarrow{D}$ tensor

$$\begin{aligned} (\Delta d)^2 &= d_{xx}^2 + d_{yy}^2 + d_{zz}^2 \\ &= \frac{2}{3}(D^2 + 3E^2). \end{aligned} \quad (86)$$

The widths and intensities of the five fine structure lines for the case of spin S = 5/2

$$\begin{aligned} |\pm 5/2\rangle &\leftrightarrow |\pm 3/2\rangle \\ |\pm 3/2\rangle &\leftrightarrow |\pm 1/2\rangle \\ |1/2\rangle &\leftrightarrow |-1/2\rangle \end{aligned} \quad (87)$$

depend upon the inner product $(\Delta d)^2$ and the correlation time τ_c.

Burlamacchi (307) calculated $\Delta H/(\Delta d)^2$ and the intensity as a function of $\omega_o\tau_c$ for these transitions, as shown by the graphs in Figure 10. We see from these plots that for $\omega\tau_c \ll 1$, the total intensity converges to the central $|½\rangle \leftrightarrow |-½\rangle$ transition. For $\omega_o\tau_c \gg 1$, the other transitions broaden beyond detectability and only the $|½\rangle \leftrightarrow |-½\rangle$ transition is observed. Near $\omega_o\tau_c \simeq 1$, the central transition reaches a maximum width, and near $\omega_o\tau_c \simeq$ 1.5 to 2, the $|+3/2\rangle \leftrightarrow |\pm ½\rangle$ transition partially contributes to the observed spectra. Burlamacchi and coworkers (276,306,307,364) confirmed this theory experimentally with Fe^{3+} and Mn^{2+} in various solvents over a wide range of temperatures. Also see (107,162,234,365).

Reed et al (366) calculated linewidths and transition probabilities for the equation (87) transitions as eigenvalues and eigenvectors, respectively, of a T_2 relaxation matrix for Mn^{2+}

$$\frac{4}{15}(D^2 + 3E^2)\begin{pmatrix} A & D & E & 0 & 0 \\ D & B & 0 & F & 0 \\ E & 0 & C & 0 & E \\ 0 & F & 0 & B & D \\ 0 & 0 & E & D & A \end{pmatrix} = 0 \quad (88)$$

where the rows and columns are labeled by $|M_s\rangle$ = $|2\rangle$, $|1\rangle$, $|0\rangle$, $|-1\rangle$, and $|-2\rangle$, and the matrix

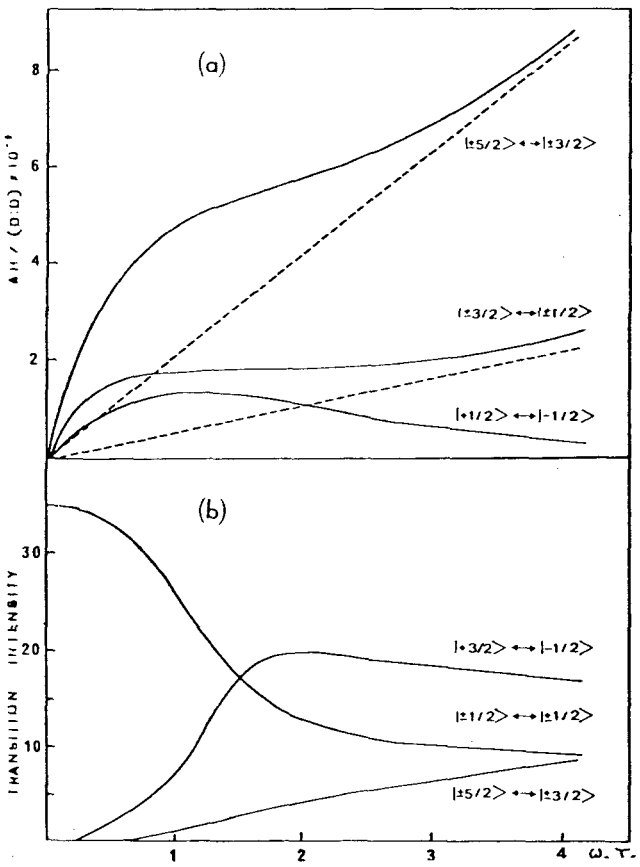

Figure 10. Theoretical curves for a sextet electron spin state as a function of $\omega\tau_0$: (a) linewidth ΔH normalized relative to the zero-field term D, (b) transition intensity (from reference 307). Transition is indicated on each curve.

elements are

$$A = -2(6J_o + 12J_1 + 7J_2)$$
$$B = -(3J_0 + 18J_1 + 23J_2)$$
$$C = -4(2J_1 + 7J_2)$$
$$D = 2\sqrt{10}J_1 \qquad (89)$$
$$E = 6\sqrt{5}J_2$$
$$F = 18J_2$$
$$J_n = \tau_c/(1 + n^2\omega^2\tau_c^2)$$

Graphs of calculated widths and intensities versus τ_c resembled those in Figure 10.

Reed et al also found that an individual Mn^{2+} solution spectrum was compatible with a range of τ_c and $(D^2 + 3E^2)$ values, but that the simultaneous fit of X-band (9.1 GHz) and Q-band (35 GHz) spectra from the same solution corresponded to unique τ_c and $(D^2 + 3E^2)$ values. Table 9 summarizes their results for various Mn^{2+} complexes. Rubinstein et al (367) obtained similar results with aquo Mn^{2+} using ^1H NMR.

Levanon et al (368) performed X-band and Q-band studies of a series of ferric aqueous complexes $[Fe(H_2O)_nF_{6-n}]^{3-n}$ that had linewidths which varied with values of n. They determined equilibrium constants for the various complexes.

Maniv et al (264) studied Mn^{2+} in single crystals of Cs_2HfCl_6 and Cs_2ZrCl_6 and found fine structure effects analogous to the solution cases described above. These arise from jumps of the D-tensor axis of the $(MnCl_6)^{3-}$ group between three equivalent crystallographic cubic axes defined by the missing Cl^- ions in the XCl_6 octahedron that would be present in the absence of the manganese. Sharma (100) found that the linewidth of Gd^{3+} in rare earth trifluorides varies with the individual fine structure transition.

XVIII. SPIN LABELS

Nitroxides and other stable free radicals called spin labels have been used as probes to monitor molecular motion in liquids and polymers and especially in biological systems. Spin labels are attached to or occupy positions near active sites in proteins or other molecules. They produce spectra which are sensitive to the anisotropies of the local environment and to the extent that molecular motion averages these anisotropies. Variations in linewidths and shapes can serve as indicators of changes in the environment. In addition, the hyperfine coupling constant A and the g-factor are sensitive to the extent to which the environment is hydrophobic or hydrophilic.

The most commonly used spin labels are nitroxides which contain an •NO group with an unpaired electron on the nitrogen atom. Examples of the molecular configuration of spin labels are peroxylamine disulfonate (I), and piperidone-1-oxyl (II) which has been used, for example, in its 2,2,6,6, tetramethyl form. They exhibit a three-line hyperfine pattern from the $I = 1$ nucleus of ^{14}N, and both

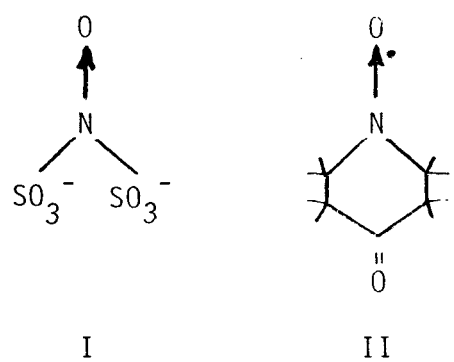

I II

A and g are generally anisotropic with principal directions oriented so that x is along the N-O band direction, z is perpendicular to the •N-O plane, and y is in this plane and perpendicular to x. The principal values of the A and g tensors are obtained by computer simulation for high viscosity solutions. Typical values are

$$\begin{aligned} g_x &= 2.008 \qquad A_x = 5.5\text{G} \\ g_y &= 2.006 \qquad A_y = 4.0\text{G} \\ g_z &= 2.003 \qquad A_z = 30.0\text{G} \end{aligned} \tag{90}$$

Freed (369) analyzed motional effects on nitroxide spectra in the slow-tumbling region where the correlation time τ_c is between 10^{-9} and 10^{-6} s (see section XII). When the rotational diffusion constant D is isotropic, τ_c is approximated by the Einstein-Stokes relationship, equation (55). For peroxylamine disulfonate, D is axially symmetric, with $D_\parallel$ along the y direction and $D_\perp$ in the xz plane of the coordinate system defined above. The rotational correlation time τ_R, which is analogous to τ_c in equation (57) is given by (369)

$$\tau_R = \frac{1}{6\sqrt{D_\parallel D_\perp}} \tag{91}$$

The value of τ_R and the ratio $D_\parallel/D_\perp$ for a particular temperature may be obtained by evaluating the factors A, B, and C of equation (71) as explained by Freed (253).

Mason et al (370) treated the case of a nitroxide radical undergoing rapid rotation about a single bond with the correlation time $\tau_{R\parallel}$ while it is attached to a macromolecule which is slowly reorienting with the correlation time $\tau_{R\perp}$. They simulated spectra for various rates of reorientation. Benton and Lynden-Bell (371) studied a similar case.

Livshits (372) calculated lineshapes for the slow rotational region, τ between 10^{-7} and 10^{-4}s, and obtained expressions for the widths of each hyperfine component. He plotted shifts of the $m = \pm 1$ lines from their rigid lattice positions as a function of the correlation time. Samples in this slow rotational region are conveniently studied by an adiabatic fast-passage method and with the aid of an ELDOR spectrometer.

Van et al (373) presented a general treatment of motional averaging at the rapid motion limit $\tau_c \ll 10^{-8}$ s. After developing the general formalism, they considered specific examples of preferential rotation about a given axis, the nitroxide principal axes in particular; wobble, regarded as a random walk over a spherical region near the pole characterized by $\theta < \theta_o$; and motion restricted to oscillations in a plane.

Libertini et al (191,192) treated spin labels diffused into fluid bilayer regions of biological membranes containing lipids which tend to be oriented normal to the membrane plane. They applied the distribution function

$$\rho_{(\theta)} = \sin\theta \exp[(\theta-\theta_o)^2/2\sigma^2] \tag{92}$$

For small σ, this is a Gaussian distribution, but for large σ it becomes sinusoidal. Gaffney and McConnell (374) used both equation (92) and the more complex distribution function

$$\rho'_{(\theta,\phi)} = \sin\theta \exp[(\theta-\theta_o)^2/2\sigma^2] \exp[\phi^2/2\sigma^2] \tag{93}$$

in their study of phospholipid membranes.

Tenny et al (375) employed a stochastic method to analyze the spin label results from rat liver and hepatoma mitochondrial lipids. They found that the logarithm of the correlation time increased linearly with the reciprocal temperature.

Shiotani and Sohma (376,377) studied molecular motions in polymethylmethacrylate in the temperature range 77 to 500 K with the use of spin labels. The powder-pattern lineshape was partially averaged between 360 and 410 K and was isotropic above 470 K. They analyzed the temperature dependence of linewidths and shapes to obtain correlation times and activation energies.

Nagamura and Woodward (378) used a nitroxide radical probe embedded in a polymer matrix to monitor molecular motion. In contrast to its use in biological applications, the probe was only weakly held by, rather than bound to, the polymer chains. Poly (trans 1,4 butadiene) produced a broad unsymmetric spectrum at low temperatures which froze polymer motion, and a sharp triplet at high temperatures which allowed the probe molecules to rotate freely. Bullock et al (379) also studied spin-labeled polymers.

The spin probes discussed so far have been ordinary radical doublet states ($S = 1/2$). Biradicals (347) and triradicals (380-383) have also been used as spin probes. These multiple radicals have, respectively, triplet-singlet and quartet-doublet zero-field splittings which are sensitive to the anisotropies of the environment. As a result, linewidth and shape variations occur which serve to monitor such anisotropies and any motions that cause averaging.

Table 11 summarizes some of the recent work on spin labels.

XIX. AQUEOUS ENVIRONMENTS

The dielectric constant ϵ of water has large real and imaginary parts

$$\epsilon = \epsilon' - j\epsilon'' \tag{94}$$

As a result, dielectric losses modulate the magnetic

Table 11. Representative Spin-label Reports with Linewidth and Lineshape Data

Spin label	Substrate	Solvent	Comments	References
di-t-butyl nitroxide	—	adamantane	180 – 250 K	384
5-doxylstearic acid	egg lecithin	—	orientational distribution model	191,192
di-t-butyl nitroxide	—	solution	activation energy, correlation time	344
imidoxyl	—	glycerol, polyethylene	anisotropy studied	345
maleimide, tanol	hemoglobin	glycerol	—	385
nitroxide, doxyl	polymer	DMF	anisotropic rotation theory	370
steroid	membranes	—	rapid anisotropic motion	373
cholestanol	membranes	—	Redfield relaxation theory	374
tetramethyl-4-hydroxyl piperidine-1-oxyl	polymethyl methacrylate	—	see text	376,377
nitroxide	—	glycerol, polyethylene	^{14}N,^{15}N HFS	345,346
nitroxide	rod-shaped	supercooled H_2O	240 – 288 K	343
tanone, imidoxyl	plastic	—	inhomogeneous, ELDOR	386
nitroxide	—	supercooled H_2O	240 – 288 K	343
nitroxide	rod-shaped	—	simulated spectra	371
nitroxide	polystyrene	toluene, cyclobenzene, chloronaphthalene	rotating chain ends	379
12-nitroxide-stearic acid	hepatoma lipids	—	stochastic	375
nitroxyl	—	decalin, ethylbenzene	anisotropy, additional broadening	387
tanol, HDA	—	sec-butylbenzene	ELDOR	385,388,389
tetramethyl-4-piperidinol-1-oxyl	butadiene	heptane, toluene	activation energy	378

losses of paramagnetic spins in aqueous solutions. The effect is analogous to the modulation of magnetic losses by conduction losses in the ESR of metals (126,390).

For aqueous samples that are thin compared with the wavelength, for example, 0.2 mm for the X-band, the dielectric loss effect is negligible and the lineshape is absorptive. For thick samples, such as 1 cm for the X-band, the shape is a mixture of absorption and dispersion. This was demonstrated (391) by measurements at 8.84 GHz where the dielectric constant is

$$\epsilon = \epsilon_o(63 - j31.8) \qquad (95)$$

Most solution studies employ thin aqueous solution cells for which this effect is not very important.

To explain the results, a calculation was made (391) of the lineshape for a thin (0.1-mm) layer of spins bathed on each side by a 4.65-mm-thick planar layer of dielectric constant $\epsilon_o(63 - j50)$. It was found that the shape changed from absorptive through dispersive to absorptive of the opposite phase as the dielectric constant of the spin-containing region varied from $\epsilon_o(23 - j50)$ to $\epsilon_o(43 - j50)$ to $\epsilon_o(63 - j50)$. The sample dielectric constant that gave a purely dispersive signal varied with the imaginary part of the dielectric constant of the bathing solution. The authors applied their technique to the study of biological membranes.

XX. TOPICS OMITTED

This review by no means exhausts all aspects of lineshapes and widths in electron spin resonance. Significant material could have been added to all the topics covered, and in some cases theory was hardly touched upon. A number of important topics were not covered, such as the ESR of ordered systems and phase transitions, acoustic and conduction ESR, Jahn Teller effects, liquid crystals, triplet states, and optical excitation.

ACKNOWLEDGEMENT

The authors wish to thank Mr. Willie Zimmerman for his help in organizing the tables and references in this article.

References

[1] C.P. Poole, *Electron Spin Resonance,* Wiley-Interscience, New York, 1967.

[2] C. Kittel and E. Abrahams, *Phys. Rev.* **90,** 238 (1953).

[3] E.R. Menzel and J.R. Wasson, *J. Phys. Chem.* **79,** 366 (1975).

[4] I. Svare, *Phys. Rev. A* **138,** 1718 (1965).

[5] M. Rakos, O. Bartko, and M. Jelvina, *Czech. J. Phys.* **23,** 394 (1973).

[6] E. Buluggiu, A. Dall'olio, G. Dascola, and V. Varacca, *Phys. Rev.* **179,** 289, (1969).

[7] R.F. Wenzel, *Phys. Rev. B* **1,** 3109 (1970).

[8] D.E. O'Reilly and T. Tsang, *Phys. Rev.* **128,** 2639 (1962); **131,** 2522 (1963).

[9] D.P. Lin and L. Kevan, *J. Phys. Chem.* **81,** 1498 (1977).

[10] J.H. Van Vleck, *Phys. Rev.* **74,** 1168 (1948).

[11] H. Panepucci and H.A. Farach, *Med. Phys.* **4,** 46 (1977).

[12] T.Z. Huang, R.P. Taylor, and Z.G. Soos, *Phys. Rev. Lett.* **28,** 1054 (1972).

[13] J. Janecka, H.M. Vyas, and M. Fujimoto, *J. Chem. Phys.* **54,** 3229 (1971).

[14] H. Hinkel, H. Port, H. SixL, M. Schwoerer, P. Reineker, and D. Richardt, *Chem. Phys.* **31,** 101 (1978).

[15] S. Dattagupta and M. Blume, *Phys. Rev. B* **10,** 4540, 4551 (1974).

[16] R.C. Hughes and Z.G. Soos, *J. Chem. Phys.* **52,** 6302 (1970).

[17] C.M. Bogan and L.D. Kispert, *J. Chem. Phys.* **57,** 3109 (1972).

[18] J.R. Byberg, S.J.K. Jensen, and B.S. Kirkegaard, *J. Chem. Phys.* **61,** 138 (1974).

[19] K.K. Ermakovich, V.N. Lazukin, V.M. Talarintsev, and I.V. Chepeleva, *Fiz. Tverd. Tela* (Leningrad) **19,** 3488 (1977), tr. p. 2040.

[20] U. Ya. Zevin, *Sov. Phys. Solid State* **3,** 662 (1961).

[21] D. Schoemaker and J.L. Kolopus, *Phys. Rev. B* **2,** 1148 (1970).

[22] D. Schoemaker, *Phys. Rev. B* **7,** 786 (1973).

[23] M.V. Krishnamurthy, *J. Chem. Phys. Solids* **33,** 164s (1972).

[24] G. Sperlich, P.H. Zimmermann, and G. Keller, *Z. Phys.* **270,** 267 (1974).

[25] J.C.M. Henning and J.H. den Boef, *Phys. Rev. B* **18,** 60 (1978).

[26] R. Boscaino, M. Brai, and I. Ciccarello, *Phys. Rev. B* **13,** 2798 (1976).

[27] R. Boscaino, M. Brai, and I. Ciccarello, Eighteenth Ampère Congress, Nottingham, 139 (1974).

[28] R. Boscaino, M. Brai, I. Cicarello, and G. Contrino, *Phys. Lett. A* **46,** 190 (1973).

[29] A.A. Bugai, V.M. Maksimenko, and L.A. Suslin, *Phys. Status Solidi K* **19,** 149 (1973).

[30] A.A. Bugai, M.D. Glinchuk, M.F. Delgen, and V.M. Maksimenko, *Phys. Status Solidi B* **44,** 199 (1971).

[31] A.A. Bugai, B.K. Krulikovskii, V.M. Maksimenko, and A.B. Roitsin, *Sov. Phys. JETP* **40,** 377 (1975).

[32] P.J. Bendt, *Phys. Rev. B* **2,** 4375 (1970).

[33] A.A. Bugai, O.G. Duliv, B.K. Krulinkovskii, and A.B. Roitsin, *Phys. Status Solidi B* **57,** K15 (1973).

[34] A.A. Bugai, P.T. Levkovskii, and V.M. Maksimenko, *Ukr. Fiz. Zh.* **15,** 508 (1971), Russian edition.

[35] R.S. Saraswat and G.C. Upreti, *Physica B* **92,** 253 (1977).

[36] L. Shia and G. Kokoszka, *J. Chem. Phys.* **60,** 1101 (1974).

[37] A.G. Petrova, A.V. Rakov, V.P. Yarigin, E.N. Ivanov, and Yu. I. Pashintsev, *Fiz. Tekh. Poluprovodn* **5,** 1140 (1971).

[38] G.C. Upreti, *J. Phys. Chem. Solids* **35,** 461 (1974).

[39] B.A. Sastry and G.S. Sastry, *Indian J. Pure Appl. Phys.* **12,** 632 (1974).

[40] B.A. Sastry and G.S. Sastry, *Physica (Utrecht)* **54,** 20 (1971).

[41] S.K. Hoffman and J.R. Goslar, *Acta Phys. Pol. A* **48,** 707 (1975).

[42] D. Arbilly, G. Deutscher, E. Grunbaum, R. Orbach, and J.T. Suss, *Phys. Rev. B* **12,** 5068 (1975).

[43] P. Urban, D. Davidov, B. Elschner, T. Plefka, and G. Sperlich, *Phys. Rev. B* **12,** 72 (1975).

[44] S.A. Marshall, T. Marshall, and R.A. Serway, *Phys. Status Solidi* **48,** 165 (1978).

[45] R. Elschner and G. Weimann, *Solid State Commun.* **9,** 1935 (1971).

[46] J. Dietrich, *Phys. Status Solidi* **73,** K57 (1976).

[47] J.P. Wolfe and C.D. Jeffries, *Phys. Rev. B* **4,** 731 (1971).

[48] M.M. Abraham, L.A. Boatner, C.B. Finch, and R.W. Reynolds, *Phys. Rev. B* **3,** 2864 (1971).

[49] B. Bleaney, R.P. Penrose, and B.I. Plumpton, *Proc. R. Soc. London, Ser. A* **198,** 406 (1949).

[50] D.W. Posener, *Aust. J. Phys.* **12,** 184 (1959).

[51] T.G. Castner, *Phys. Rev.* **115,** 1506 (1952).

[52] H.A. Farach and H. Teitelbaum, *Can. J. Phys.* **45,** 2913 (1967).

[53] M.W.P. Strandberg, *Ann. Phys.* **77,** 174 (1973).

[54] A.M. Stoneham, *J. Phys. D.* **5,** 670 (1972).

[55] T.S. Al'tshuler, I.A. Garifullin, E.G. Kharakhash'yan, and L.F. Shatrukov, *Sov. Phys. Solid State* **14,** 2213 (1973).

[56] M.D. Kemple and H.J. Stapleton, *Phys. Rev. B* **5,** 1668 (1972).

[57] R. Freedman and D.R. Fredkin, *Phys. Rev. B* **11,** 4847 (1975).

[58] D.C. Langreth, D.L. Cowan, and J. W. Wilkins, *Solid State Commun.* **6,** 131 (1968).

[59] G.F. Reiter and J.P. Boucher, *Phys. Rev. B* **11,** 1823 (1975).

[60] R. Servant and E. Palangie, *Mol. Relax. Inter. Process.* **13,** 231 (1978).

[61] K.M. Salikhov, A.B. Doctorov, Yu. N. Molin, and K.I. Zamaraev, *J. Magn. Reson.* **5,** 189 (1971).

[62] K.M. Salikhov, A.T. Nikitaev, G.A. Senyukova, and K.I. Zamaraev, *Teor. Eksp. Khim.* **7,** 503 (1971).

[63] B.N. Misra, S.D. Sharma, and S.K. Gupta, *Acta Phys. Pol. A* **49,** 35 (1976).

[64] M. Abkowitz and A.R. Monahan, *J. Chem. Phys.* **54,** 811 (1971).

[65] M. Abkowitz and A.R. Monahan, *J. Chem. Phys.* **58,** 2281 (1973).

[66] C.P. Cheng and S.I. Weissman, *J. Phys. Chem.* **80,** 872 (1976).

[67] V.N. Parmon, A.T. Nikitaev, G.M. Zhidomirov, and K.I. Zamaraev, *Zh. Strukt. Khim.* **13,** 566 (1972).

[68] J. Heinzer, *Mol. Phys.* **22,** 167 (1971).

[69] J. Heinzer, *J. Magn. Reson.* **13,** 124 (1974).

[70] P.J. Krusic and P. Meakin, *Chem. Phys. Lett.* **18,** 347 (1973).

[71] C. Cusumano and G.J. Troup, *Phys. Status Solidi B* **65,** 655 (1974); **66,** 47 (1974).

[72] L.A. Shul'man and G.A. Podzyarei, *Sov. Phys. Solid State* **14,** 1521 (1972).

[73] N.M. Atherton, *Chem. Phys. Lett.* **23,** 454 (1973).

[74] K. Shimoda, G. Moshuk, H.D. Conner, P. Colume, and M. Szwarc, *Chem. Phys. Lett.* **14,** 396 (1972).

[75] C.R. Mao and R.W. Kreilick, *Mol. Phys.* **31,** 1447 (1976).

[76] V.B. Stryukov, L.A. Shul'man, A.V. Zvarykina, and D.N. Fedutin, *Sov. Phys. Solid State* **16,** 187 (1974).

[77] K. Murakami and A. Kawamori, *Solid State Commun.* **22,** 47 (1977).

[78] J.C.M. Henning and J.P.M. Damen, *Phys. Rev. B* **3,** 3852 (1971).

[79] M.I. Belinskii, *Fiz. Tverd. Tela (Leningrad)* **20,** 887 (1978).

[80] M.I. Belinskii and B.Ya. Kuyavskaya, *Fiz. Tverd. Tela (Leningrad)* **18,** 1822 (1976).

[81] M.I. Belinskii, B.S. Tsukerblat, and A.V. Ablov, *Sov. Phys. Solid State* **16,** 639 (1974).

[82] B.S. Tsukerblat and M.P. Chobanu, *Sov. Phys. Solid State* **18,** 1232 (1976).

[83] R.C. Thompson, Y. Hoyano, and C.R. Schwerdtfeger, *Solid State Commun.* **23,** 633 (1977).

[84] P.A. Fedders, *Phys. Rev. B* **3,** 2352 (1971).

[85] J.H. Pifer and R.T. Longo, *Phys. Rev. B* **4,** 3797 (1971).
[86] R.E. Walstedt and L.R. Walker, *Phys. Rev. B* **11,** 3280 (1975).
[87] D. Davidov, C. Retorri, R. Orbach, A. Dixon, and E.P. Chock, *Phys. Rev. B* **11,** 3546 (1975).
[88] I. Svare and G. Seidel, *Phys. Rev. A* **134,** 172 (1964).
[89] M. Tanaka and Y. Kondo, *J. Phys. Soc. Jpn.* **38,** 1539 (1975); **40,** 35 (1976).
[90] T.G. Castner, and M.S. Seehra, *Phys. Rev. B* **4,** 38 (1971).
[91] B.N. Misra, S.K. Gupta, *Acta Phys. Pol. A* **43,** 317 (1973).
[92] A.D. Toy, T.D. Smith, and J.R. Pilbrow, *J. Chem. Soc. A,* 2600 (1970).
[93] G.D. Sootha, G.K. Padam, and S.K. Gupta, *Acta Phys. Pol. A* **50,** 641 (1976).
[94] T.A. Kennedy, S.H. Choh, and G. Seidell, *Phys. Rev.* **82,** 3645 (1970).
[95] Z.G. Soos, T.Z. Huang, J.S. Valentine, and R.C. Hughes, *Phys. Rev. B* **8,** 993 (1973).
[96] A.A. Samokhvalov, V.S. Babushkin, V.G. Bamburov, and N.I. Lobachevskaya, *Sov. Phys. Solid State* **13,** 2530 (1972).
[97] P.K. Schwob, M. Tachiki, and G.E. Everett, *Phys. Rev. B* **10,** 165 (1974).
[98] K. Baberschke and Y. von Spalden (unpublished results).
[99] H.R. Neukomm and R. Hauger, *Z. Phys. B* **20,** 323 (1975).
[100] V.K. Sharma, *J. Chem. Phys.* **54,** 496 (1971).
[101] N.L.H. Liu, K.J. Lingi, and R. Orbach, *Phys. Rev.* **14,** 4087 (1976).
[102] J.P. Boucher, *Phys. Rev. B* **4,** 3819 (1971).
[103] C.W. Myles, *Phys. Rev. B* **15,** 5326 (1977).
[104] C. Cusumano and L.L. Vivoli, *Physica* (Utrecht) **86-88B,** 1289 (1977).
[105] A.V. Lazuta and S.V. Maleev, *Sov. Phys. JETP* **38,** 1038 (1974).
[106] B.N. Misra, S.K. Gupta, and S.D. Sharma, *Ind. J. Pure Appl. Phys.* **10,** 483, 737 (1972).
[107] B.N. Misra, S.K. Gupta, and S.D. Sharma, *Nuovo Cimento Soc. Ital. Fis.* **5,** 145, 567 (1971); **7,** 498 (1973); *B* **19,** 129 (1974).
[108] B.N. Misra and S.K. Gupta, *Nuovo Cimento Soc. Ital. Fis. B* **18,** 285 (1973).
[109] A.M. Portis, *Techn. Note* 1, Sarah Mellon Scaife Radiation Laboratory, Univ. of Pittsburgh, 1955 (unpublished).
[110] A.M. Portis, *Phys. Rev.* **91,** 1071 (1953).
[111] C.P. Poole and H.A. Farach, *Relaxation in Magnetic Resonance,* Academic Press, New York, 1971.
[112] R.E. Coffman, *J. Phys. Chem.* **79,** 1129 (1975).
[113] P.R. Cullis, *J. Magn. Reson.* **21,** 397 (1976).
[114] I.T. Semenov and M.S. Fogel'son, *Sov. Phys. Semicond.* **9,** 1264 (1975).
[115] I.B. Baumberg, D.M. Daraseliya, and T.I. Sanadze, *Sov. Phys. JETP* **35,** 553 (1972).
[116] A.S. Epifanov and A.A. Manenkov, *Sov. Phys. JETP* **33,** 976 (1971).
[117] A.A. Bugai, *Sov. Phys. Solid State* **4,** 2218 (1963).
[118] O.P. Zhidkov, V.O. Muromtsev, I.G. Akhvlediani, S.N. Safronov, and V.V. Kopylov, *Sov. Phys. Solid State* **9,** 1095 (1967).
[119] B.E. Vugmeister, V.L. Gokhman, and V. Ya. Zevin, *Sov. Phys. Solid State* **14,** 2280 (1973).
[120] C. Mailer, T. Sarna, H.M. Swartz, and J.S. Hyde, *J. Magn. Reson.* **25,** 205 (1977).
[121] M. Bowman, L. Kevan, R.N. Schwartz, and B.L. Bales, *Chem. Phys. Lett.* **22,** 19 (1973).
[122] L. Kevan and L.D. Kispert, *Electron Spin Double Resonance Spectroscopy,* Wiley Interscience, N.Y. 1976.
[123] P.C. Taylor, J.F. Baugher, and H.M. Kriz, *Chem. Rev.* **75,** 203 (1975).
[124] B. Bleaney, *Philos. Mag.* **42,** 441 (1951).
[125] B. Bleaney, *Proc. Phys. Soc. A* **63,** 407 (1950); **75,** 621 (1960).
[126] N. Bloembergen and T.J. Rowland, *Acta Met. I,* **731** (1953); *Phys. Rev.* **97,** 1679 (1955).
[127] R.H. Sands, *Phys. Rev.* **99,** 1222 (1975).
[128] L.S. Singer, *J. Chem. Phys.* **23,** 379 (1955).
[129] R.P. Kohin and C.P. Poole, *Bull. Am. Phys. Soc. II.* **3,** 8 (1961).
[130] D.E. O'Reilly, *J. Chem. Phys.* **29,** 1188 (1958).
[131] J.W. Searl, R.C. Smith, and S.J. Wyard, *Proc. Phys. Soc.* **74,** 491 (1959); *Arch. Sci. Fasc. Spec.* **13,** 2036 (1960), Ninth Colloque Ampère.
[132] J.W. Searl, R.C. Smith, and S.J. Wyard, *Proc. Phys. Soc.* **78,** 1174 (1961).
[133] F.K. Kneubuhl, *J. Chem. Phys.* **33,** 1074 (1960).
[134] S.M. Blinder, *J. Chem. Phys.* **33,** 748 (1960).
[135] R. Lefebvre, *J. Chem. Phys.* **33,** 1826 (1960).
[136] H. Sternlicht, *J. Chem. Phys.* **33,** 1128 (1960).
[136a] F.K. Kneubuhl and B. Natterer, *Helv. Phys. Acta,* **34,** 710 (1961).
[137] A.C. Chirkov and A.A. Kokin, *Sov. Phys. JETP* **39,** 964 (1960).
[137a] N.W. Lord and S.M. Blinder, *J. Chem. Phys.* **34,** 1694 (1961).
[138] R. Neiman and O. Kivelson, *J. Chem. Phys.* **35,** 156 (1961).
[138a] F.K. Kneubuhl, W.S. Koski, and W.S. Caughey, *J. Am. Chem. Soc* **83,** 1607 (1961).
[139] E.L. Cochran, F.J. Adrian, and V.A. Bowers, *J. Chem. Phys.* **34,** 1161 (1961).
[140] K. Hever, *Jenaer. Jahrbuch* **I,** 223 (1961).
[141] J.A. Ibers and J.D. Swalen, *Phys. Rev.* **127,** 1914 (1962).
[142] H.R. Gersmann and J.O. Swalan, *J. Chem. Phys.* **36,** 322 (1962).
[143] F.G. Wakim and A. Nolle, *J. Chem. Phys.* **37,** 3000 (1962).
[144] T. Vänngård and P. Aasa, *Paramagn. Reson.* **2,** 509 (1963).
[145] P. Kottis and R. Lefebvre. *J. Chem. Phys.* **39,** 393 (1963).
[146] Ya.S. Lebedev, *Zh. Strukt. Khim.* **4,** 19 (1962).
[147] J.A. Weil and H.G. Hecht, *J. Chem. Phys.* **38,** 281 (1963).
[148] D.E. Hughes and T. J. Rowland, *Can. J. Phys.* **42,** 209 (1964).
[149] V.S. Korolkov and A.K. Potpovich, *Opt. Spektrosk.* **16,** 251 (1964).
[150] T.S. Johnson and H.G. Hecht, *J. Mol. Spect.* **17,** 98 (1965).
[151] M.M. Malley, *J. Mol. Spec.* **17,** 210 (1965).
[152] M. Iwasaki, K. Toriyama and B. Eda, *J. Chem. Phys.* **42,** 63 (1965).
[153] R. Lefebvre and J. Maruani, *J. Chem. Phys.* **42,** 1480 (1965); **34,** 2035 (1961).
[154] G. Schoffa and G. Bürk, *Phys. Status Solidi B* **8,** 557 (1965).
[155] C. Chachaty and J. Maruani, *Can. J. Chem.* **44,** 2681 (1966).
[156] M. Lardon and H.H. Gunthard, *J. Chem. Phys.* **44,** 2010 (1966).
[157] M. Iwasaki, *J. Chem. Phys.* **45,** 990 (1966).
[158] M. Che, J. Demarquay and C. Naccache, *J. Chem. Phys.* **51,** 5177 (1969).
[159] J.A.R. Coope, *Chem. Phys. Lett.* **3,** 539 (1969).
[160] J. Maruani, J.A. Coope, and C.A. McDowell, *Mol. Phys.* **18,** 165 (1970).
[161] L.E. Mohrmann, B.B. Garrett, and W.B. Lewis, *J. Chem. Phys.* **52,** 535 (1970).
[162] B.B. Garrett and L.O. Morgan, *J. Chem. Phys.* **44,** 890 (1966); B.B. Garrett, K. DeArmond, and H.S. Gutowsky, ibid. 3393 (1966).
[163] R. Aasa and T. Vänngård, *J. Chem. Phys.* **52,** 1612 (1970).
[164] N.Ya. Shteinshneider and G.M. Zhidomirov, *Teor. Eksp. Khim.* **6,** 651 (1970), tr. p. 531.
[165] F.O. Tsay, H.B. Gray, and J. Danon, *J. Chem. Phys.* **54,** 3760 (1971).
[166] P. Mailhe, A. Briguet, and B. Tribollet, *J. Phys. Chem. Solids* **32,** 2639 (1971).
[167] S. Moriuchi and J. Sohma, *Mem. Fac. Engrg.,* Hokkaido Univ., **2,** 147 (1972).
[168] S. Moriuchi and J. Sohma, *Mol. Phys.* **21,** 369 (1971).
[169] C.P. Poole and H.A. Farach, *Theory of Magnetic Resonance,* Wiley, New York, 1972.
[170] J.S. Shaffer, H.A. Farach, and C.P. Poole, *Phys. Rev. B* **13,** 1869 (1976).

[171] C. Hauser, *Helv. Phys. Acta* **45,** 683 (1972).
[172] C. Hauser and B. Renaud, *Phys. Status Solidi A* **10,** 161 (1972).
[173] M.G. Blazha and A.B. Roitsin, *Sov. Phys. Solid State* **14,** 416 (1972).
[174] P.A. Narayana and K.V.L.N. Sastry, *J. Chem. Phys.* **57,** 1805 (1972).
[175] F.C. Herring, C.A. McDowell, and J.C. Tait, *J. Chem. Phys.* **57,** 4564 (1972).
[176] W.V. Sweeney, D. Coucouvanis, and R.E. Coffman, *J. Chem. Phys.* **59,** 369 (1973).
[177] S. Hirokawa, *J. Phys. Soc. Jpn.* **35,** 12 (1973); **37,** 897 (1974).
[178] S. Hirokawa, *Mol. Phys.* **36,** 29 (1978).
[179] V.A. Gaponenko, L.V. Mosina, and Yu.V. Yablokov, *J. Struct. Chem.* **14,** 442 (1973).
[180] M.G. Blazha and A.B. Roitsin, *Sov. Phys. Solid State* **16,** 327 (1974).
[181] M.Ya. Shcherbakova and V.E. Istamin, *Phys. Status Solidi B* **67,** 461 (1975).
[182] M. Jinguji, K.C. Lin, C.A. MacDowell, and P. Raghunathan, *J. Chem. Phys.* **65,** 3910 (1976).
[183] I.V. Ovchinnikov and V.N. Konstantinov, *Sov. Phys. Solid State* **18,** 859 (1976).
[184] C.O. Clark, C.P. Poole, and H.A. Farach, *J. Phys. C* **11,** 769 (1978).
[185] D. Niarchos, A. Kostikos, A. Simopoulos, D. Coucouvanis, D. Piltingsrud, and R.E. Coffman, *J. Chem. Phys.* **68,** 4411 (1978).
[186] P.C. Taylor and P.J. Bray, *J. Magn. Reson.* **2,** 305 (1970).
[187] M.G. Blazha, A.A. Bugai, V.M. Maksimenko, and A.B. Roitsin, *Sov. Phys. Solid State* **14,** 1779 (1973).
[188] A. Isomoto, H. Watari, and M. Kotani, *J. Phys. Soc. Jpn.* **29,** 1571 (1970).
[189] J.R. Pilbrow, *Mol. Phys.* **16,** 307 (1969).
[190] N.N. Korst, A.N. Kuznetsov, A.V. Lazarev, and E.P. Gordeev, *Teor, Eksp. Khim.* **8,** 51 (1972).
[191] L.J. Libertini, C.A. Burke, P.C. Jost, and O.H. Griffith, *J. Magn. Reson.* **15** 460 (1974).
[192] L.J. Libertini, A.S. Waggoner, P.C. Jost, and O.H. Griffith, Proc. Nat. Acad. Sci. USA **64,** 13 (1969).
[193] C.A. McDowell, H. Nakajima, and P. Raghunathan, *Can. J. Chem.* **48,** 805 (1974).
[194] C.A. McDowell, P. Raghunathan, and P.C. Tait, *J. Chem. Phys.* **59,** 5858 (1973).
[195] P.H. Kasai and D. McLeod, *J. Chem. Phys.* **55,** 1566 (1971).
[196] P.H. Kasai, W. Weltner, and E.B. Whipple, *J. Chem. Phys.* **42,** 1120 (1965); **44,** 2581 (1966).
[197] L.B. Knight, W.C. Easley, and W. Weltner, *J. Chem. Phys.* **54,** 1610 (1971).
[198] R. Hentschel, J. Schlitter, H. Sillescu, and H.W. Spiess, *J. Chem. Phys.* **68,** 56 (1978).
[199] R.C. Nicklin, H.A. Farach, and C.P. Poole, *J. Chem. Phys.* **65,** 2998 (1976).
[200] R. Aasa, *J. Chem. Phys.* **52,** 3919 (1970).
[201] H.W. DeWijn and R.F. Van Balderen, *J. Chem. Phys.* **46,** 1381 (1967).
[202] G. Vincow and P.M. Johnson, *J. Chem. Phys.* **39,** 1143 (1963).
[203] G.S. Owen and G. Vincow, *J. Chem. Phys.* **54,** 368 (1971).
[204] P.C. Taylor and P.J. Bray, *J. Phys. Chem. Solids* **33,** 43 (1972).
[205] R.C. Nicklin, C.P. Poole, and H.A. Farach, *J. Chem. Phys.* **58,** 2579 (1973).
[206] R.C. Nicklin, J.K. Jonestone, R.G. Barnes, and D.R. Wilder, *J. Chem. Phys.* **59,** 1652 (1973).
[207] B.L. Bales, M.K. Bowman, L. Kevan, and R.N. Schwartz, *J. Chem. Phys.* **63,** 3008 (1975).
[208] B.L. Bales, J. Helbert, and L. Kevan, *J. Phys. Chem.* **78,** 221 (1974).
[209] D.L. Griscom, *Phys. Rev.* (submitted for publication).
[210] D.L. Griscom, E.J. Friebele, and G.H. Sigel, *Solid State Commun.* **15,** K169 (1978).
[211] A. Carnevale, G.E. Peterson, and C.R. Kurkjian, *J. Noncryst, Solids* **22,** 269 (1976).
[212] G.E. Jellison, P.J. Bray, and P.C. Taylor, *Phys. Chem. Glasses* **17,** 35 (1976).
[213] G.E. Peterson, C.R. Kurkjian, and A. Carnevale, *Phys. Chem. Glasses* **15,** 52 (1974).
[214] R.S. Abdrakhmanov and T.A. Ivanova, *J. Mol. Struct.* **46,** 229 (1978).
[215] R.S. Abdrakhmanov, T.A. Ivanova, and V. Yu. Petukhov, *Fiz. Khim. Stekla* **2,** 489 (1976).
[216] R. Berger, *Verres Refract.* **32,** 172 (1978).
[217] M. Kumeda, Y. Nakagaki, M. Suzuki, and T. Shimizu, *J. Noncryst. Solids* **29,** 15 (1978).
[218] L.D. Bogomolova, V.A. Jackkin, V.N. Lazukin, T.K. Pavlushkima, and V.A. Shmuckler, *J. Noncryst. Solids* **28,** 375 (1978).
[219] J.F. Anderson and R. Ullman, *J. Chem. Phys.* **47,** 2178 (1967).
[220] P.W. Atkins and D. Kivelson, *J. Chem. Phys.* **44,** 169 (1966).
[221] D. Kivelson, *J. Chem. Phys.* **27,** 1087 (1957); **33,** 1094 (1960).
[222] D. Kivelson, *J. Chem. Phys.* **45,** 1324 (1966).
[223] D. Kivelson, M.G. Kivelson, and I. Oppenheim, *J. Chem. Phys.* **52,** 1810 (1970).
[224] N.N. Korst and L.I. Antsiferova, *Usp. Siznauk.* **126,** 67 (1978).
[225] S. Moriuchi and J. Sohma, *Mem. Fac. Engrg.,* Hokkaido Univ., 335 (1974).
[226] G.E. Reiter, *Phys. Rev. B* **9,** 3780 (1974).
[227] D. Sames, *Z. Phys.* **198,** 71 (1967).
[228] H. Sillescu and D. Kivelson, *J. Chem. Phys.* **48,** 3493 (1968).
[229] R.C. Wilson and D. Kivelson, *J. Chem. Phys.* **44,** 154, 4440 (1966).
[230] H. Sillescu, *J. Chem. Phys.* **54,** 2110 (1971).
[231] P.W. Atkins and B.P. Hills, *Mol. Phys.* **29,** 761 (1975).
[232] H.L. Friedman, L. Blum, and G. Yue, *J. Chem. Phys.* **65,** 4396 (1976).
[233] K. Hensen, W.O. Riede, H. Sillescu, and A. von Wittgenstein, *J. Chem. Phys.* **61,** 4365 (1974).
[234] B.N. Misra, S.D. Sharma, and S.K. Gupta, *Indian J. Pure Appl. Phys.* **13,** 61 (1975).
[235] S. Alexander, A. Beram, and Z. Luz, *Mol. Phys.* **27,** 441 (1974).
[236] L. Antsiferova and N. Korst, *Chem. Phys. Lett.* **15,** 439 (1972).
[237] L. I. Antsiferova, A.V. Lazarev, and V.B. Stryukov, *Zh. Eksp. Teor. Fiz. Pis. Red.* **12,** 108 (1970).
[238] A. Beram, Z. Luz, and S. Alexander, *J. Chem. Phys.* **64,** 432 (1976).
[239] S.A. Goldman, G.V. Bruno, and J.H. Freed, *J. Phys. Chem.* **76,** 1858 (1972).
[240] J.B. Pederson, *J. Chem. Phys.* **57,** 2680 (1972).
[241] N.N. Korst and T.N. Khazanovich, *Sov. Phys. JETP* **18,** 1049 (1964).
[242] S.A. Goldman, G.V. Bruno, and J.H. Freed, *J. Chem. Phys.* **59,** 3071 (1973).
[243] S.A. Goldman, G.V. Bruno, C.F. Polbaszek, and J.H. Freed, *J. Chem. Phys.* **56,** 716 (1972).
[244] L.P. Hwang, C.F. Anderson, and H.L. Friedman, *J. Chem. Phys.* **62,** 2098 (1975).
[245] J.L. Monroe and H.L. Friedman, *J. Chem. Phys.* **66,** 955 (1977).
[246] S. Clough and F. Poldy, *J. Phys. C* **6,** 1953 (1973).
[247] S. Clough, M. Starr, and M.D. McMillan, *Phys. Rev. Lett.* **25,** 839 (1970).
[248] R.B. Davidson and I. Miyagawa, *J. Chem. Phys.* **52,** 1727 (1970), **57,** 1815 (1972).
[249] C.A. McDowell, P. Raghunathan, and K. Shimokoshi, *J. Chem. Phys.* **58,** 114 (1973).
[250] C.A. McDowell and K. Shimokoshi, *J. Chem. Phys.* **60,** 1619 (1974).

[251] J. Maruani, C.A. McDowell, H. Nakajuma, and P. Raghunathan, *Mol. Phys.* **14,** 349 (1968).
[252] N.V. Vugman, M.F. Elia, and R.P.A. Muniz, *Mol. Phys.* **30,** 1813 (1975).
[253] J.H. Freed, *J. Chem. Phys.* **43,** 1710 (1965).
[254] P.J. Krusic, P. Meakin, and J.P. Jesson, *J. Phys. Chem.* **75,** 3438 (1971).
[255] D. Raoux, *J. Phys. Chem. Solids* **36,** 359 (1975).
[256] L.L. Chase, *Phys. Rev. B* **2,** 2308 (1970).
[257] S. Clough, J.R. Hill, and M. Punkkinen, Eighteenth Ampère Congress, Nottingham, 289 (1974).
[258] W. Kaminski, *Z. Naturforsch.* Teil A **25,** 639 (1976).
[259] J.A. McMillan and S.A. Marshall, *J. Chem. Phys.* **48,** 467 (1968).
[260] J. Stankowski, A. Dezor, B. Sczaniecki, and J.M. Janik, *Phys. Status Solidi K* **16,** 167 (1973).
[261] J. Subramanian and P.T. Narasimhan, *J. Chem. Phys.* **56,** 2572 (1972).
[262] F.J. Adrian, E.L. Cochran, and V.A. Bowers, *J. Chem. Phys.* **59,** 56 (1973).
[263] J. Isoya, J.A. Weil, and R.F.C. Claridge, *J. Chem. Phys.* **69,** 4876 (1978).
[264] S. Maniv, A. Reuveni, and Z. Luz, *J. Chem. Phys.* **66,** 2285 (1977).
[265] K.I. Zamaraev, R.F. Khairutdinov, and J.R. Miller, *Chem. Phys. Lett.* **57,** 311 (1978).
[266] Y. Ayant, *J. Phys.* **37,** 219 (1976).
[267] Y. Ayant, R. Besson, and A. Salvi, *J. Phys.* **36,** 571 (1975).
[268] O.A. Anisimov, A.T. Nikitaev, K.I. Zamaraev, and Yu. N. Molin, *Teor. Eksp. Khim.* **7,** 556 (1971).
[269] C.P. Poole and J.F. Itzel, *J. Chem. Phys.* **41,** 287 (1964).
[270] C.P. Poole and D.S. MacIver, *Adv. Catal.* **17,** 223 (1966).
[271] J.P. Lloyd and G.E. Pake, *Phys. Rev.* **92,** 1576 (1953); **94,** 576 (1954).
[272] J. Haupt, I. Kramer, and W. Müller-Warmuth, Eleventh Colloque Ampère, 709 (1962).
[273] H. Levanon, S. Charbinsky, and Z. Luz, *J. Chem. Phys.* **53,** 3056 (1970).
[274] H. Levanon, S. Charbinsky, and Z. Luz, *J. Chem. Phys.* **66,** 955 (1977).
[275] L. Burlamacchi, G. Martini, and M. Romanelli, *J. Chem. Phys.* **59,** 3008 (1973).
[276] L. Burlamacchi, G. Martini, and E. Tiezzi, *J. Phys. Chem.* **74,** 3980 (1970).
[277] E.F. Strother, H.A. Farach, and C.P. Poole, *Phys. Rev. A* **4,** 2079 (1971).
[278] G.P. Vishnevskaya, F.M. Gumerov, and B.M. Kozyrev, *Teor. Eksp. Khim.* **11,** 162 (1975).
[279] K. Tanemoto and T. Nakamura, *Jpn. J. Appl. Phys.* **17,** 1561 (1978).
[280] K. Murakami, S. Nambe, N. Kishimoto, K. Masuda, and K. Gamo, *Appl. Phys. Lett.* **30,** 300 (1971).
[281] K. Murakami, S. Nambe, N. Kishimoto, K. Masuda, and K. Gamo, *J. Appl. Phys.* **49,** 2401 (1978).
[282] G.M. Muha and J. Sakamoto, *J. Chem. Phys.* **68,** 1432 (1978).
[283] T. Shiga, A. Lund, and P. Xinell, *Int. J. Rad. Phys. Chem.* **3,** 131 (1971).
[284] L.A. Shul'man, G.A. Podzyarei, and T.A. Nachal'naya, *Ukr. Fiz. Sh.* **16,** 371 (1971).
[285] E.E. Stel'nitskii, S.I. Bakula, et al, "Synthetic Diamond", *in Naukova Dumka* (Kiev) **4,** 14 (1977).
[286] K. Sugihara, *J. Phys. Soc. Jpn.* **38,** 1061 (1975).
[287] K. Morigaki, S. Toyotomi, and Y. Toyotomi, *J. Phys. Soc. Jpn.* **31,** 511 (1971).
[288] M. Kumeda, Y. Jinno, and T. Shimizu, *Phys. Status Solidi B* **81,** K71 (1977).
[289] M. Onda and K. Morigaki, *J. Phys. Soc. Jpn.* **34,** 1107 (1973).
[290] E.J. Friebele, L.K. Wilson, and D.L. Kinser, *J. Am. Chem. Soc.* **55,** 164 (1972).
[291] T. Muramoto, *J. Phys. Soc. Jpn.* **35,** 921 (1973).
[292] M. Teodorescu, *Rev. Roum. Phys.* **22,** 73 (1977).
[293] E. Chovino, R. Sardos, and R. Chastanet, *C.R. Acad. Sci.* **273,** 557 (1971).
[294] E. Burzo and M. Balanescu, *Solid State Commun.*, **28,** 693 (1978).
[295] G. Koopmann, K. Baberschke, and U. Engel, *Solid State Commun.* **12,** 997 (1973).
[296] T-Trong Nguyen, L.B. Chiu, P.P. Elliston, A.M. Stewart, and K.N.R. Taylor, *Physica* (Amsterdam) B + C **86-88,** 181 (1977).
[297] R.G. Kooser, W.V. Volland, and J.H. Freed, *J. Chem. Phys.* **50,** 5243 (1969).
[298] L. Burlamacchi and M. Romanelli, *Chem. Phys. Lett.* **10,** 59 (1971).
[299] G.E. Pake and T.R. Tuttle, *Phys. Rev. Lett.* **3,** 423 (1959).
[300] S.K. Rengan, M.P. Khakhar, B.S. Prabhananda, and B. Venkataraman, *Proc. Nucl. Phys. & Solid State Phys. Symp. BARC* (Bombay) **3,** 231 (1972).
[301] J. Leblond, P. Papon, and J. Korringa, *Phys. Rev. A* **4,** 1539 (1971).
[302] J. Leblond and J. Uebersfeld, *Phys. Rev. A* **4,** 4 (1971).
[303] J. Leblond, J. Uebersfeld, and K. Korringa, *Phys. Rev. A* **4,** 1532 (1971).
[304] R.C. Wilson and R.J. Myers, *J. Chem. Phys.* **64,** 2208 (1976).
[305] K.H. Hausser, *Z. Elek.* **65,** 636 (1961).
[306] M. Romanelli and L. Burlamacchi, *Mol. Phys.* **31,** 115 (1976).
[307] L. Burlamacchi, *J. Chem. Phys.* **55,** 1205 (1971).
[308] R. Poupko, *J. Magn. Reson.* **12,** 119 (1973).
[309] S.V. Cheema and M.J.A. Smith, *J. Phys. C* **4,** 1231 (1971).
[310] G. Gewinner, L. Kubler, J.J. Koulmann, and A. Jaegle, *Phys. Status Solidi B* **59,** 395 (1975); **70,** 595 (1975).
[311] R. Servant, *C.R. Acad. Sci.* **280,** 447 (1975).
[312] A.R. Boate, J.R. Morton, and K.F. Preston, *J. Phys. Chem.* **80,** 2954 (1976).
[313] S. Hasegawa and S. Yazaki, *Thin Solid Films* **55,** 15 (1978).
[314] L. Kubler, G. Gewinner, J.J. Koulmann, and A. Jaegle, *Phys. Status Solidi B* **78,** 149 (1976).
[315] D.J. Lepine, *Phys. Rev. B* **2,** 249 (1970).
[316] S. Nagai, S. Ohnishi, and I. Nitta, *Chem. Phys. Lett.* **13,** 379 (1972).
[317] K. Drager, *Z. Naturforsch.* **31,** 622 (1976).
[318] D.L. Huber and M.S. Seehra, *Phys. Chem. Solids* **36,** 723 (1975).
[319] M.S. Seehra and R.P. Gupta, *Phys. Rev. B* **9,** 197 (1974).
[320] B.N. Misra P. Giquere and G.R. Sharp, *J. Chem. Phys.* **66,** 1758 (1973).
[321] J. Stasz, *Acta Phys. Pol. A* **51,** 524 (1976); **52,** 831 (1977).
[322] B. Clerjaud, A. Kuhn, and B. Lambert, Sixteenth Congress Ampère, Bucharest, 1009 (1970).
[323] F.J. Owens, *J. Chem. Phys.* **57,** 2349 (1972).
[324] T. Grouchulski, K. Leibler, and A. Sienkiewicz, *Phys. Status Solidi K* **47,** 169 (1978).
[325] E. Dormann, R.D. Hogg, D. Hone, and V. Jaccarino, *Physica C.*, Proc. Int. Conf. Magnetism, **86-88,** 1183 (1976).
[326] A.M. Stoneham, K.A. Muller, and W. Berlinger, *Solid State Commun.* **10,** 1005 (1972).
[327] A. Nazarian, Y.H. Shing, D. Walsh, and G. Donnay, *Solid State Commun.* **24,** 213 (1977).
[328] H. Feichtinger, J. Welti, and A. Gechwandtner, *Solid State Commun.* **27,** 867 (1978).
[329] M.S. Seehra and T.G. Castner, *Phys. Kond. Mater.* **7,** 185 (1968).
[330] A. Kawamori, S. Matsura, and H. Abe, *J. Phys. Soc. Jpn.* **29,** 1173 (1970).
[331] H.J. Stapleton and K.L. Brower, *Phys. Rev.* **178,** 481 (1969).
[332] I. Ursu and E. Burzo, *J. Magn. Reson.* **8,** 274 (1972).
[333] C. Vittoria, P. Lubitz, and V. Ritz, *J. Appl. Phys.* **49,** 4908 (1978).

[334] A.I. Filippov and I.S. Donskaya, *Dokl. Akad. Nauks. SSR* **205,** 138 (1972).
[335] A.I. Filippov and I.S. Donskaya, *Dokl. Akad. Nauks. SSR* **214,** 1124 (1974).
[336] A.I. Filippov and I.S. Donskaya, *Zh. Fiz. Khim.* **47,** 1271 (1973).
[337] R.N. Rogers and G.E. Pake, *J. Chem. Phys.* **33,** 1107 (1960).
[338] D. Hoel and D. Kivelson, *J. Chem. Phys.* **62,** 4535 (1975).
[339] T.E. Eagles and R.E.D. McClung, *Can. J. Phys.* **53,** 1432 (1975).
[340] F. Barbarin and J.P. Germain, *J. Phys.* **36,** 475 (1975).
[341] J.H. Freed, G.V. Bruno, and C.F. Polnaszeh, *J. Phys. Chem.* **75,** 3385 (1971).
[342] L.D. Kispert and F. Myers, *J. Chem. Phys.* **56,** 2623 (1972).
[343] M.K. Ahn, *J. Chem. Phys.* **64,** 134 (1976).
[344] G. Poggi and C.S. Johnson, *J. Magn. Reson.* **3,** 436 (1970).
[345] V.B. Stryukov and E.G. Rozantsev, *Teor. Eksp. Khim.* **7,** 209 (1971).
[346] V.B. Stryukov, P.A. Stunzhas, and S. Tikirillov, *Chem. Phys. Lett.* **25,** 453 (1974).
[347] P.L. Nordio, *Chem. Phys. Lett.* **6,** 250 (1970).
[348] S. Radhakrishna, B.V.R. Chowdari, and A.K. Viswanath, *J. Magn. Reson.* **16,** 199 (1974).
[349] N.S. Angerman and R.B. Jordan, *J. Chem. Phys.* **54,** 837 (1971).
[350] G.R. Luckhurst, M. Setaka, and J. Subramanian *Mol. Phys.* **32,** 1299 (1976).
[351] B.N. Misra, S.K. Gupta and S.D. Sharma, *Nuovo Cimento Soc. Ital. Fis.* **42,** 205 (1977).
[352] R. Poupko and Z. Luz, *J. Chem. Phys.* **57,** 3311 (1972).
[353] W.W. Schmidt and K.G. Breitschwerdt, *Chem. Phys. Lett.* **27,** 527 (1974).
[354] Yu.A. Bobrov, A.D. Krivospitskii, and C.K. Chirkin, *J. Struct. Chem.* **14,** 761 (1973).
[355] J.R. Bolton and A. Carrington, *Mol. Phys.* **5,** 161 (1962).
[356] J.H. Freed, G.K. Fraenkel, *J. Chem. Phys.* **37,** 1156 (1962).
[357] J.H. Freed, P.H. Rieger, and G.K. Fraenkel, *J. Chem. Phys.* **37,** 1881 (1962).
[358] E. DeBoer and A.P. Praat, *Mol. Phys.* **8,** 291 (1964).
[359] M. Iwaizumi and T. Isobe, *Bull. Chem. Soc. Jpn.* **38,** 1547 (1965).
[360] F.W. Pijpers, M.R. Arick, B.M.P. Hendriks, and E. De Boer, *Mol. Phys.* **22,** 781 (1971).
[361] S.A. Al-Baldawi and T.E. Gough, *Can. J. Chem.* **48,** 2098 (1970).
[362] S.A. Al-Baldawi and T.E. Gough, *Can. J. Chem.* **49,** 2059 (1971).
[363] J.H. Freed and G.K. Fraenkel, *J. Chem. Phys.* **39,** 326 (1962).
[364] L. Burlamacchi, G. Martini, M.F. Ottaviani, and M. Romanelli, *Adv. Mol. Relax. Inter. Proc.* **12,** 145 (1978).
[365] U. Kaufmann, A. Rauber, and J. Schneider, *Phys. Status Solidi B* **74,** 169 (1976).
[366] G.H. Reed, J.S. Leigh, and J.E. Pearson, *J. Chem. Phys.* **55,** 3311 (1971).
[367] M. Rubinstein, A. Baras, and Z. Luz, *Mol. Phys.* **20,** 67 (1971).
[368] H. Levanon, G. Stein, and Z. Luz, *J. Chem. Phys.* **53,** 876 (1970).
[369] J.H. Freed, in *Spin Labeling: Theory and Applications,* L.J. Berliner, Ed., Academic Press, New York, 1976, Chapter 3.
[370] R.P. Mason, C.F. Polnaszek, and J.H. Freed, *J. Phys. Chem.* **78,** 1324 (1974).
[371] J.E. Benton and R.M. Lynden-Bell, *J. Chem. Soc.,* Faraday Trans. 2, **71,** 807 (1975).
[372] V.A. Livshits, *J. Magn. Reson.* **24,** 307 (1976).
[373] S.P. Van, G.B. Birrell, and O.H. Griffith, *J. Magn. Reson.* **15,** 444 (1974).
[374] B.J. Gaffnery and H.M. McConnell, *J. Magn. Reson.* **16,** 1 (1974).
[375] J.R. Tenny, D.L. Cowan, R.L. Bernay, M.L. Vorbeck, and A.P. Martin, *Biophy. Struct. Mechanism* **4,** 111 (1978).
[376] M. Shiotani and J. Sohma, *Prog. Polymer Phys. Japan* **17,** 505 (1974).
[377] M. Shiotani and J. Sohma, *Polymer J.* **9,** 283 (1977).
[378] T. Nagamura and A.E. Woodward, *J. Polym. Sci.* **14,** 275 (1976).
[379] A.T. Bullock, G.H. Cameron, and N.K. Reddy, *J. Chem. Soc.,* Faraday Trans 1, **74,** 727 (1978).
[380] G. Kothe, *Mol. Phys.* **33,** 147 (1977).
[381] G. Kothe, A. Naujok, and E. Ohmes, *Mol. Phys.* **32,** 1215 (1976).
[382] G. Kothe and E. Ohmes, *J. Mol. Struct.* **46,** 481 (1978).
[383] G.R. Luckhurst and C. Zannoni, *J. Magn. Reson.* **23,** 275 (1976).
[384] J.A. Berman, R.N. Schwartz, and B.L. Bales, *Mol. Cryst. Liq. Cryst.* **28,** 51 (1973).
[385] J.S. Hyde and D.D. Thomas, *Ann. N.Y. Acad. Sci.* **222,** 689 (1974).
[386] T. Kirillov, M.A. Kozhushner, and V.B. Stryukov, *Chem. Phys.* **17,** 243 (1976); *Zh. Eksp. Teor. Fiz.* **68,** 2249 (1975).
[387] A.N. Kuznetsov, A.Y. Volkov, V.A. Livshits, and A.T. Nirzoian, *Chem. Phys. Lett.* **26,** 369 (1974).
[388] J.S. Hyde and L. Dalton, *Chem. Phys. Lett.* **16,** 568 (1972).
[389] J.S. Hyde, M.D. Smigel, L.R. Dalton, and L.A. Dalton, *J. Chem. Phys.* **62,** 1655 (1975).
[390] F.J. Dyson, *Phys. Rev.* **98,** 349 (1955).
[391] G. Gillberg-La Force and R. Conley-La Force, *J. Chem. Phys.* **58,** 5402 (1973).